NATIONAL TRANSPORTATION SAFETY BOARD

Office of Research and Engineering
Materials Laboratory Division
Washington, D.C. 20594

October 16, 2002

MATERIALS LABORATORY FACTUAL REPORT Report No. 02-083

A. ACCIDENT

Place	:	Belle Harbor, New York
Date	:	November 12, 2001
Vehicle	:	Airbus A300-600, N14053
NTSB No.	:	DCA02MA001
Investigator	:	Brian Murphy, AS-40

B. COMPONENTS EXAMINED

Vertical stabilizer longitudinal attachment lugs and adjacent skin panel structure.

C. ACCIDENT SUMMARY

On November 12, 2001, at approximately 0917 EST, American Airlines flight 587, an Airbus A-300-600, N14053, crashed into a neighborhood in Belle Harbor, New York, several minutes after taking off from Kennedy International Airport. The airplane was on a scheduled flight to Santo Domingo, Dominican Republic. All 260 persons aboard the airplane were fatally injured, as were 5 on the ground.

D. DETAILS OF THE EXAMINATION

This report documents the fractographic examination of the six vertical stabilizer longitudinal attachment lugs and the adjacent structure as primarily completed at the Safety Board's materials laboratory. Materials Laboratory Factual Report 02-077 contains information regarding the overall construction and visual examination of the damage for the entire vertical stabilizer and adjacent fuselage, rudder, and rudder hinges.

Parties to the examination were the Federal Aviation Administration (FAA), the Bureau Enquetes – Accidents (BEA), Airbus Industrie, American Airlines (AA), and the Airline Pilots Association (APA). Participants in the fractographic examination of the components included:

Matthew R. Fox, Ph.D.
Materials Engineer
NTSB

Carl R. Schultheisz, Ph.D.
Materials Research Engineer
NTSB

Larry B. Ilcewicz, Ph.D.
National Resource Specialist,
Composites
FAA

Jean-Francois Berthier
Investigator, Engineering Department
BEA

Armand Gastellu
Technical Advisor
Airbus Industrie

Erhard Winkler
Engineer
Airbus Industrie

Klaus Harnisch-Scheuermann
Failure Analyst
Airbus Industrie

Jochen Müller
Composites Technology
Airbus Industrie

Robert S. Stegeman
Senior Structures Engineer
AA

Michael Hair
Structural Engineer
AA

Shannon Hankins
APA

James Reeder, Ph.D.
Research Engineer
NASA Langley

James H. Starnes, Jr. Ph.D.
Chief Engineer for Structures and
Materials
NASA Langley

1. Construction

The primary attachment locations for the vertical stabilizer are six composite lugs (longitudinal lugs) that connect by bolts to six metal clevis fittings on the fuselage. Three longitudinal lugs extend from the lower end of each of the two vertical stabilizer skin panels. At the thickest point, the longitudinal lugs are approximately 1.62 inches, 2.48 inches, and 2.17 inches thick for the forward, center, and aft lugs, respectively. The thickness of each lug decreases as plies are dropped in the lug-to-skin transition area. The longitudinal attachment lugs are a solid carbon-fiber reinforced polymer (CFRP) laminate composed of T300 carbon fibers in a Hexcel 913[1] epoxy matrix. The laminate includes both unidirectional tape and eight-harness satin woven fabric layers in the construction. The zero-degree fibers of the fabric and tape layers in the composite are oriented parallel to the stringers and aft spar, which is at an angle of 33.3 degrees aft relative to vertical. The +45-degree fibers are oriented 11.7 degrees forward relative to vertical.

[1] At the time the accident airplane was manufactured, the epoxy used in the vertical stabilizer was CIBA 913C, made by Ciba-Geigy Ltd., of Switzerland. Ciba-Geigy sold their composites business to Hexcel Corporation in 1996.

Each lug contains two separate pieces that are cured separately before the final assembly. In the final assembly, the outer precured half is laid down, followed by the skin layers, then the inner precured half, the compensation layers, the rib 1 attach flange, the stringer inner flange (tape) layers, and the stringer module layers. A schematic view of the typical assembly cross-section is shown in figure 1. After the assembly is cured, the lug attach bolt holes are core-drilled out.

The rudder is a single-segment wedge-shaped design with curved leading edge fairings. The wedge consists of left and right skin panels with a single spar at the forward side. The rudder skin panels and spar are sandwich composite panels having a nomex honeycomb core with glass-fiber reinforced polymer (GFRP) and CFRP face sheets.

2. Examination Procedure

Fracture features were examined visually and magnified using an optical stereoscope and scanning electron microscopy (SEM). Before the SEM examination, the specimens were generally cleaned with soapy water in an ultrasonic cleaner followed by rinsing in water then alcohol. Some of the translaminar fracture surfaces were examined uncoated using SEM. Then the samples were coated with a thin layer of gold and palladium before further examination using SEM.

3. Vertical Stabilizer Attachment Lugs and Adjacent Structure

A detailed description of the damage at each of the longitudinal attachment lugs is provided below. The right rear, right forward, and left forward lugs had translaminar fractures that intersected the lug bore. Based on the non-destructive inspections described in Materials Laboratory Factual Report 02-078, the left aft and the left forward lug areas had interlaminar fractures that were present in the structure above the lugs up to approximately 46 inches and 52 inches, respectively, along the zero-degree fiber direction. Except for these two areas, interlaminar fractures were limited to the lug area below the rib 1 (lower rib) fasteners or to within 4 inches of a translaminar fracture. The damage to the lugs is described right to left, aft to forward, with the translaminar fractures detailed first followed by any interlaminar fractures.

3.1. Right Aft

An overall view of the right aft lug upper fracture area on the vertical stabilizer is shown in figure 2. A piece of rib 1 was displaced downward and was covering the inboard side of the fracture surface on the forward leg of the lug. Another view of the right forward lug is shown in figure 3 as viewed from the left after sectioning from the vertical stabilizer. The fracture surfaces intersected the lug attach hole. The lower piece of the lug was not recovered and was missing.

Views of the translaminar fracture surfaces on the aft and forward legs of the right aft lug are shown in figures 4 and 5. The translaminar fracture surfaces had a rough

appearance consistent with fracture primarily under tensile loading. Fractures on each leg of the lug were on different translaminar planes, and the change in planes occurred near the center of the lug thickness. On the aft leg, the outboard side of the fracture was in a plane nearly perpendicular to the zero-degree fiber direction, and the inboard side of the fracture was in a plane approximately parallel to the 45-degree fiber direction. On the forward leg, the outboard side of the fracture was in a plane approximately parallel to the zero-degree fiber direction, and the inboard side of the fracture was in a nearly horizontal plane. Bearing damage was observed at the bore surface near both fracture surfaces, as indicated in figures 4 and 5.

Some interlaminar cracks were observed above the fracture. Black arrows in figures 4 and 5 indicate the largest cracks visible at the outer surface. These cracks intersected the translaminar fracture where the fracture plane changed. The interlaminar cracks visible at the surface were limited to the lug region below rib 1.

The fracture surfaces were sectioned from the remainder of the lug by cutting at the locations indicated in figure 3. To further facilitate the examination using SEM, specimens RA2 and RA3 were separated along the interlaminar plane that corresponded to the change of plane in the translaminar fracture. This was accomplished by using a screwdriver to pry open the interlaminar cracks indicated in figures 4 and 5. A “-1” and “-2” were added to the specimen labels to indicate the outboard and inboard specimens, respectively. (For example, the inboard portion of specimen RA2 was labeled RA2-2).

The translaminar fracture surface on the aft leg of the lug, specimens RA2-1 and RA2-2, were examined using SEM. For fibers oriented in the zero-degree direction, the fibers typically showed radial fracture patterns over their fracture surfaces, consistent with overstress fracture under tensile loads. Similar fracture features were observed throughout the fracture surface. Typical fracture surface features for fibers oriented in the zero-degree orientation are shown in figure 6. Unlabeled arrows in figure 6 indicate the direction of crack propagation within individual fibers. The direction of fracture was sampled from fibers in many locations, and the general direction of fracture was to the left of aft.

Near the inboard side of specimen RA2-1 (near the center of the lug thickness), the –45-degree fibers were oriented nearly perpendicular to the fracture surface. In this area, these fibers typically showed radial fracture patterns over their fracture surfaces, consistent with overstress fracture under tensile loads. Typical fracture surface features for fibers oriented in the –45-degree orientation in this area are shown in figure 7. Unlabeled arrows in figure 7 indicate the direction of crack propagation within individual fibers. The direction of fracture was sampled from fibers in several locations, and the general direction of fracture was slightly to the right of aft.

The translaminar fracture surface on the inboard portion of the forward leg of the lug, specimen RA3-2, was examined using SEM. Fiber ends in many areas of the fracture surface were bent to the right, consistent with post-fracture contact with rib 1. For fibers that were not bent and were oriented in the zero-degree direction, the fibers typically showed radial fracture patterns over their fracture surfaces, consistent with overstress

fracture under tensile loads. Similar fracture features were observed throughout the fracture surface. Typical fracture surface features for fibers oriented in the zero-degree orientation are shown in figure 8. Unlabeled arrows in figure 8 indicate the direction of crack propagation within individual fibers. The direction of fracture was sampled from fibers in many locations, and the general direction of fracture was nearly directly forward.

The interlaminar fracture on specimen RA2-1 of the aft leg was examined using SEM. Examination of the surface using the SEM showed evidence of hackles[2] associated with shearing deformation at the fracture surface (Mode II or Mode III fracture). However, the SEM examination did not find any microscopic indications of fatigue, such as matrix rollers[3], widespread abrasion or striations on exposed fiber surfaces or their imprints.

3.2. Right Center

Overall views of the fracture at the right center lug area are shown in figures 9 and 10. The fracture occurred in the vertical stabilizer structure above the lug bore. Translaminar fractures occurred in the skin and the lug build-up layers primarily in a slightly curved plane perpendicular to the zero-degree fiber direction at a location up to approximately 12 inches above the lug attach bolt centerline. As shown in figure 11, the translaminar fracture appeared rough, consistent with fracture from tensile loading. The stringer module structure and stringer outer flange layers, as indicated in figure 9, remained with the upper piece. Rib 1 fastener holes near the lower end of the stringer module and outer flange layers were torn out as shown in the detail in figure 9. The holes are shown numbered aft to forward for reference. The holes for the fasteners that remained with the lower piece were torn out primarily in a downward direction. For holes 2 to 8, the hole was torn out at the lower forward side in a direction parallel to the zero-degree fiber direction, followed by a downward tearout. The material between holes 8 and 9 was torn out and remained attached to the lower piece. A piece of the upper leg of the rib 1 attach angle also remained with the lower piece, as shown in figure 10. Some layers of tape pulled out from the lower piece near the forward side and remained with the upper piece.

The translaminar fracture surface on the lower piece was examined using SEM on two specimens, labeled specimens RC1 and RC2 in figure 9. For fibers oriented in the zero degree direction, the fiber ends generally showed radial fracture patterns over their fracture surfaces, consistent with overstress fracture under tensile loads. Similar fracture features were observed throughout the fracture in areas RC1 and RC2. Typical fracture

[2] Matrix fracture features called hackles indicate a significant component of shear (Mode II or Mode III) across the fracture surface. Hackles are formed as a result of fairly regularly spaced matrix microcracks along planes of maximum tension (at an angle to the main fracture surface), which eventually join together. Hackles typically form as plates perpendicular to adjacent fibers, with the edges of the hackles pointing generally in the direction opposite the shear tractions acting on the surface. Because of the nature of shearing deformation, hackles on mating fracture surfaces point in opposite directions, which means that the orientation of the hackles cannot necessarily be used to determine the overall direction of crack propagation, since the coalescence of the matrix microcracks can occur along one of two opposite pathwaysWhen hackles break off from a surface, they leave scoop marks that are called scallops.

[3] Matrix rollers are the remains of hackles that have broken off and been deformed or abraded into small cylinders by repeated shear loading.

surface features for fibers oriented in the zero-degree orientation are shown in figures 12 and 13 for each area. The area shown in figure 13 was relatively rich in resin compared to other areas on the fracture surface, and the larger areas of resin fracture are indicated in the figure. Unlabeled arrows in figures 12 and 13 indicate the direction of fracture for individual fibers. The direction of fracture was sampled from many locations in the two areas. In specimen RC2, the general direction of fracture was to the right of forward, and in specimen RC1, the direction of fracture was nearly directly forward.

3.3. Right Forward

An overall view of the right forward lug upper fracture area is shown in figure 14. Additional views of the right forward lug are shown in figures 15 to 24. The fracture surfaces intersected the lug attach hole. Most of the lower portion of the lug was missing and was not recovered, but a small amount of composite material was left in the circumferential groove between the two hat bushings that remained attached to the fuselage. The translaminar fracture surfaces had a rough appearance consistent with fracture primarily under tensile loading. A few layers near the inboard and outboard surface had translaminar fractures approximately three inches above the remaining translaminar fractures with interlaminar fractures between the translaminar fracture locations.

The aft leg of the lug is shown in figures 15 to 20. Fracture on the aft leg of the lug occurred on different planes. On the inboard and outboard sides of the aft leg, the fracture was on planes perpendicular to the zero-degree fibers along the length of the spar, and near the center of the aft leg, the fracture was on a plane approximately parallel to the 45-degree fiber direction. Near the bore surface, some fractured ends of the layers were bent to the right as shown by the black bracket in figure 15. At the aft end, some fractured ends of the layers near the center of the lug thickness were bent to the left, as shown by the white bracket in figure 16. On the right of these center layers, the fracture surface had a smooth appearance consistent with post-fracture contact damage (see arrow labeled “rubbed” in figure 15. A few layers near the inboard interlaminar fracture were not bent, as indicated in figure 15, although many adjacent layers to the right were fractured above the translaminar fracture for the indicated layer. At the aft end as indicated in figure 16, some of the fractured ends of the layers near the outboard surface were bent to the right, and some of the fractured ends of the layers near the inboard surface were bent to the left consistent with a local compressive loading.

The interlaminar fractures near the inboard and outboard sides of the aft leg were examined using SEM. Relative motions of the mating fractures were determined from the hackle directions in the epoxy matrix, and the general crack propagation direction was determined from river markings[4], also in the epoxy matrix. The results are shown in figures 17 to 20. Relative to the center layers at the time of fracture, the outer and inner layers

[4] Matrix fracture features called river marks indicate the formation of multiple microcracks that then coalesce into a larger crack. These patterns are typically found on flat areas of matrix cohesive failure as a result of tensile (Mode I) fracture in the matrix. The pattern of the coalescence of the microcracks indicates the local direction of crack propagation.

generally moved downward and aft near the hole bore surface and moved upward and aft near the aft surface.

The translaminar fracture surface on the aft leg of the lug, specimen RF2a in figure 14, was examined using SEM. For fibers oriented in the zero degree direction, the fiber fractures typically showed radial fracture patterns over their fracture surfaces as shown in figure 21 and the upper portion of figure 22, features consistent with overstress fracture under tensile loads. In some areas near the center of the lug thickness, some of the zero-degree fibers had relatively smooth fracture features with changes in the fracture plane within the fibers (called chop marks), features consistent with local fiber bending under compressive load. These areas were relatively isolated and appeared to coincide with areas where the fractured ends of layers appeared bent or damaged from the optical examination. Other zero-degree fibers in the same areas had radial fracture patterns, consistent with overstress fracture under tensile load. Figure 22 shows a view from the center of the thickness showing fibers with the different fracture features in the same view. Unlabeled arrows in figures 21 and 22 indicate the direction of fracture for individual fibers. The direction of fracture was sampled from many locations throughout specimen RF2a. For most of the fracture area, the general direction of fracture was slightly to the right of downward and aft. In the center of the thickness near the lug bore, the direction of fracture was approximately midway between the left and the downward and aft directions.

On the forward leg of the lug, the fracture surface was almost entirely on a plane that was perpendicular to the length direction of the front spar as shown in figure 23. Near the forward end, some center layers did not have transverse fractures and extended below the fracture surface to the original lug forward lower surface. The lower ends of these center layers were bent to the left and had a rubbed appearance on the right side. Red-colored deposits were observed on the fracture surface in the adjacent area.

The translaminar fracture surface on the forward leg of the lug, specimen RF1 in figure 14, was examined using SEM. For fibers oriented in the zero degree direction, the fibers typically showed radial fracture patterns over their fracture surfaces, consistent with overstress fracture under tensile loads. Similar fracture features were observed throughout the fracture surface. Typical fracture surface features for fibers oriented in the zero-degree orientation are shown in figure 24. Unlabeled arrows in figure 24 indicate the direction of fracture for individual fibers. The direction of fracture was sampled from many locations, and the general direction of fracture was slightly to the left of forward.

3.4. Left Aft

Overall views of the left aft lug area are shown in figures 25 and 26. A combination of fractures listed below allowed the lug structure to separate from the vertical stabilizer and remain attached to the fuselage after the accident, leaving a gap between the skin layers and the stringer module structures at the aft lower end of the vertical stabilizer. Ultrasonic C scans performed by NASA and by Airbus indicated that this gap was part of a continuous interlaminar fracture extending at least 2 inches forward of stringer 4 and 8 inches above rib 4. For more details of the nondestructive examination, see Materials Laboratory Factual

Report 02-078. A translaminar fracture occurred in the skin layers between the precured lug halves (about 3.5 inches above the lug bore), fracturing primarily at the rib 1 fastener row. Fractures at the upper end of the lower piece generally corresponded with the upper ends of the precured halves and the compensation layers. Interlaminar fractures occurred between the skin layers and the outer surface of the inner precured lug half and the inner surface of the outer precured lug half above the rib 1 fasteners. An interlaminar fracture also occurred primarily between the stringer outer flange (tape) layers and the stringer module layers, with some areas having interlaminar fracture between the stringer outer flange and the lug compensation layers.

In order to expose the interlaminar fracture surfaces for examination, two cuts (using a low-amplitude vibrating saw with a diamond-edged blade) were made in the upper piece from the left aft lug fracture area. The first cut was 6 inches above and parallel to rib 4 and the second just aft of stringer 4. The upper piece was cut from the exterior surface to the level of the interlaminar fracture but not through the stringer and rib structure. One fabric layer approximately 4 inches wide bridged between the two pieces along stringer 4, and that layer was cut with scissors approximately two inches below rib 4. A ribbon of zero-degree tape approximately 1/4 inch wide also bridged between the two pieces along stringer 3 at the top, and the bond between that tape and the skin section fractured as the skin section was lifted slightly from the upper piece. The mating interlaminar fracture surfaces are shown in figures 27 and 28. Additional specimens were cut for examination in the scanning electron microscope, and those specimens are shown in figures 29 and 30.

Twelve rib 1 fasteners remained attached to the lower piece from the left aft lug fracture area shown in figure 26 and were numbered aft to forward for reference. Fasteners 4, 8, and 11 are hidden in the photo by the vertical stabilizer to fuselage fairing clips. The fasteners pulled out of the lower end of the stringer module layers, as shown in figure 30. In the stringer module layers, bearing failures were observed on the lower sides of fastener holes 1, 2, 4, 10, and 11 and on the upper sides of holes 1 and 2. The stringer module layers were fractured above holes 6 to 9. Translaminar cracks intersected holes 2, 3, 4, and 10. Hole 5 was torn out downward. Below holes 3 to 5, the lower end of the stringer module layers was bent outward.

Figure 31 shows the interior surface of the skin section after cutting from the upper piece. The row of rib 1 fastener holes in the skin section is indicated in the inset photograph in this figure. The translaminar fracture in the skin intersected most of these fastener holes except for an area near the forward end, where the fracture was above holes 9 to 11.

A closer view of the surface of the translaminar fracture through the skin at the rib 1 fastener row is shown in figure 32. The fracture surface was generally rough on the inboard side and center of the fracture, consistent with an overstress fracture under tensile loading. Most of the fracture surface near the outboard side appeared smoother, and yellow-colored fibers were observed on the surface, consistent with post-fracture damage. Near the aft end of the fracture, the surface was rough from inboard to outboard, consistent with an overstress fracture under tensile loading.

The translaminar fracture surface for the skin layers on the upper piece were examined using SEM on specimens LA7a and LA5 shown in figure 29. Specimen LA7a contained both skin layers and outer precured half layers with a translaminar fracture between. When specimen LA7a was sectioned from the structure for SEM examination, it separated into two pieces, which were labeled LA7a-in for the skin layers and LA7a-out for the outer precured half layers.

Similar fracture features were observed throughout the translaminar fracture surfaces on LA7a-in and LA7a-out. For fibers oriented in the zero-degree direction, the fibers had radial fracture patterns over their fracture surfaces, consistent with overstress fracture under tensile load. The direction of fracture was sampled from many locations in the two areas. On piece LA7a-in, the general direction of fracture was approximately to the right of aft at the outside and slightly left of aft near the middle of the thickness. No zero-degree fibers were located near the outer surface. On piece LA7a-out, the general direction of fracture was slightly to the left of aft across the fracture surface.

For specimen LA5, typical translaminar fracture features for fibers oriented in the zero-degree direction are shown in figures 33 and 34. Near the inner surface, the zero-degree fibers had radial fracture patterns over their fracture surfaces, consistent with overstress fracture under tensile load. The general direction of the fracture was to the right of aft. Near the center, many of the zero-degree fibers had relatively smooth fracture features with changes in the fracture plane within the fibers (called chop marks), features consistent with local fiber bending under compressive load. Fibers with these features are indicated in figure 34. Other zero-degree fibers in the same areas had radial fracture patterns, consistent with overstress fracture under tensile load. No zero-degree fibers were located near the outer surface.

Above the rib 1 fasteners, the interlaminar fracture occurred mainly at interfaces between fabric layers and tape layers. These interlaminar fractures are described in greater detail below.

On the inner surface of the skin section shown in figure 29, the outermost ply of the inner precured lug structure remained attached to the skin layers. The edge of that ply is about 2 inches below rib 4 and below the imprint of the zero-degree tape compensation layer, which is partly visible on the stringer module structure of the upper piece shown in figure 30. A part of the next lug ply inward also remained attached to the skin section, seen as the darker layer beginning about 5 inches below rib 4 (figure 29), and there were some translaminar fractures in this fabric ply leading to the diagonal strip at forward. The next ply inward was zero-degree tape, and the imprint of that ply and five other lug plies can be seen in that area. Outside the area of the lug precured halves, the main surface visible was the innermost skin fabric ply, and the interlaminar fracture remained mainly between that ply and the stringer module structure. In addition, a second area of interlaminar fracture was found within the skin section on surfaces between three plies of zero-degree tape and the adjacent fabric layers. There were also intralaminar fractures within the tape

plies, so that the separated tape plies were localized to a column running from 2 inches aft of stringer 3 to 1 inch aft of stringer 4, and from rib 1 to above the cut made above rib 4.

On the stringer module structure, the interlaminar fracture surface that was exposed after cutting the upper piece (figure 30) was mainly between fabric layers of the stringer module structure and the inboard layer of three tape layers making up part of the stringer outer flange. Those three tape layers extended from forward of stringer 4 back to the rear spar; they ended sequentially 5 inches (125 mm) below rib 4, 2 inches (50 mm) below rib 4 and 2 inches (50 mm) above rib 4. There were additional tape layers (approximately 1.6 inches (40 mm) wide) along each stringer making up additional outer flange layers, and some of the tape layers in the area of the stringers remained attached to the stringer structure. The tape layers that were attached to the stringer structure appeared somewhat thicker toward the upper end of the fracture. There were translaminar fractures in the fabric layer making up the largest ply of the lug compensation layers, which extended from forward of stringer 4 to the rear spar, up to rib 4. The lug compensation layers were placed between the inner precured lug structure and the stringer outer flange layers. Remains of this ply can be seen forward of the midplane of stringer 3 following the contour of the lug structure down to rib 1, and in the area just below rib 4 between the area of the rear spar flange and stringer 2. This ply bridged between the two pieces and was cut with scissors at the forward area between stringers 3 and 4, about 2 inches below rib 4. The curved boundary of the adjacent compensation layer (zero-degree tape) can be seen on the fabric. That ply remained attached to the larger compensation layer beneath, and retains some imprints of fabric from lug plies and the skin surface on the mating piece. There also were translaminar fractures in the broad stringer outer flange layers, generally at the edge of the ply ending 2 inches (50 mm) below rib 4 or at the level of rib 4 itself, where there was some crimping. The last ply of the stringer outer flange can be seen extending up 2 inches (50 mm) above rib 4 in the bays between stringers 2, 3 and 4 (that ply remained attached to the mating skin layers in the areas aft of stringer 2). Farther above rib 4, the interlaminar fracture remained on the interface between the skin layers and the stringer module structure. At the lower end of the stringer module structure, interlaminar fractures were present at the midplanes of the stringer webs (fractures perpendicular to the main interlaminar fractures).

Visually, the interlaminar fracture surfaces appeared relatively smooth and were mainly confined to the matrix between plies. Over much of the surfaces, deposits (light tan or dark brown) were observed in the pockets formed where bundles in the woven fabric crossed one another or in regions where plies ended. These deposits appear to be more common higher up the part. Bundles of aramid fiber used as tracers to indicate the orientation of the fabric plies could also be seen. No visible indications of crack-arrest marks or patterns that would be associated with fatigue or other long-term pre-existing damage were observed.

Specimens were cut from the skin section (figure 29) and the stringer module structure at the lower end of the upper piece (figure 30) to facilitate microscopic examination of the interlaminar fracture surfaces using SEM. Not all cut specimens shown in figures 29 and 30 were examined using SEM, and the specimens that were examined

using SEM are described in the following text. These sections were chosen to include regions of different surface morphology associated with different plies (or their imprints) that were visible on the fracture surface. The sections were cut into specimens approximately 2 inches square using the low-amplitude vibrating saw with the diamond-edged blade or using a diamond bandsaw. Vibration during the sectioning process shook loose the tape layers associated with the second area of interlaminar fracture within the skin section. Those zero-degree tape layers also contained intralaminar (through the layer parallel to the fiber direction) fractures leading to separate columns of tape on the order of 1/4 to 1/2 inch wide. These columns were able to slide lengthwise to some extent within the skin section. Specimen LA1c and all LA3 specimens shown in figure 29 included this second interlaminar fracture and separated into three pieces after cutting. The pieces consisted of an outer piece including the original painted skin surface, a layer of zero-degree tape, and an inner piece with the inner skin layer at the main interlaminar fracture surface.

For SEM observation, all of the specimens investigated in connection with the interlaminar fractures were sputter coated with a layer of gold/palladium. The first specimen examined (specimen LA1a) was not cleaned before examination in the SEM in order to look for microscopic features that would be indicative of fatigue. No such features were observed, and the surface of specimen LA1a was covered with particles that interfered with observation in the SEM, so the remaining specimens were cleaned in deionized water in an ultrasonic cleaner.

Specimen LA1a is shown in figure 35, oriented with respect to the stringer structure. The zero-degree tape layers in the vertical stabilizer were also directed parallel to the stringers. The back surface of this specimen was the painted exterior surface of the vertical stabilizer. On the upper right side of the figure, a fabric layer is present with the main visible bundle direction at +45 degrees to the zero-degree fiber direction. That layer was the outermost layer of the precured inner lug structure. On top of that layer at the lower left, a fabric layer is present with the main visible bundles at –45 degrees to the zero-degree fiber direction; a region of damage where part of that layer was peeled away is seen in the center of the specimen. On top of those layers, a layer of zero-degree tape was present, which left scattered fibers and imprints. The damaged –45-degree fabric layer and the zero-degree tape layer were the next two plies within the outer lug structure. Examination of the surface using the SEM showed evidence of hackles associated with shearing deformation at the fracture surface (Mode II or Mode III fracture). However, the SEM examination did not reveal any microscopic indications of fatigue, such as matrix rollers, widespread abrasion or striations on exposed fiber surfaces or their imprints. The hackle features observed were generally sharp and distinct. SEM photographs were taken from several areas on the specimen surface, and an example SEM photograph from specimen LA1a (oriented along the stringers as in figure 35) is shown in figure 36.

Specimens LA1a through LA1d sampled the fracture surface of the skin section from near the center forward to the edge of the skin section. The most common surface morphology was a +45-degree fabric with zero-degree tape fibers and imprints on top. In some areas the fabric was covered by imprints of other ±45-degree fabric layers and in one case by imprints of a zero-degree/90-degree fabric layer. The hackles observed on

specimens LA1a through LA1c pointed generally upward parallel to the stringers in all locations. On specimen LA1d, the hackles pointed upward on the aft side of the specimen, where it had been in contact with the zero-degree tape lug compensation layer. On the forward edge of LA1d, which was an interface between the skin layers and the large fabric lug compensation layer, the hackles pointed downward along the stringers.

Specimens LA7a, LA7c, and LA7e were cut from the lower aft side of the skin section up to the position of rib 4. The same plies from the interior of the precured lug structure were involved in this area, and the results were similar. In specimens LA7a and LA7c, the hackles observed pointed mainly upward parallel to the stringers. The crack propagation direction appeared to be mainly aft and upward, where it could be determined. At the bottom forward area of LA7a, the crossing bundles were displaced and there were hackles in opposing directions on adjacent main bundles. In specimen LA7e, which extended out from under the zero-degree lug compensation layer (like specimen LA1d), hackles pointed upward along the stringers in the forward and aft areas, but there was a strip of zero-degree tape from the stringer outer flange just aft of the center of the specimen where hackles pointed in the opposite direction. The crack propagation direction appeared to be mainly forward.

Specimen LA3c also had hackles that pointed in different directions. That specimen was forward, above the position of rib 4, and the middle of the specimen was at the edge of the last broad stringer outer flange layer. The surface of the specimen was fabric, with primarily tape fiber and imprints on top, except at the top forward corner, which had been mated to a stringer module fabric layer. The aft third of the specimen had a thick tape overlay, and the hackles in that area pointed upward parallel to the stringers. The middle third of the specimen had thinner tape on top, and the hackles in that area pointed downward along the stringers. In the forward third of the specimen, close to the edge of the stringer module layer, the hackles primarily pointed forward, perpendicular to the stringers. The crack propagation direction was mainly forward and up where it could be observed.

Specimens LA4a and LA4b were cut from the upper part of the skin section, covering the area of the stringer 1 flange. All of specimen LA4a and the aft half of specimen LA4b were fabric with tape fibers and imprints from the stringer outer flange layers. The forward half of LA4b was +45-degree fabric, which had apparently been in contact with fabric from the stringer module structure; a damaged part of that layer left –45-degree bundles on the lower half of the specimen. In the areas with tape overlay, the hackles observed pointed generally upward parallel to the stringer. In the forward half of specimen LA4b, the hackles pointed generally down and aft in the damaged –45-degree layer at the bottom of the specimen, but the hackles pointed up and forward on the top part of the specimen, in the underlying +45-degree fabric layer.

Specimen LA5 was cut from the lower end of the skin section, and the surface of that specimen was primarily the second fabric layer from the inner precured lug structure, with tape overlay. There was also a strip at the forward edge that was the first fabric layer from the inner precured lug structure, which had been covered by the second lug fabric

layer. In general, the hackles observed were mainly pointing upward along the stringers. However, there were fracture features on this specimen that were very similar to those observed on specimen LA7a, where the crossing bundles were displaced and there were hackles in opposing directions on adjacent main bundles. An example of the crossing bundle displacement is shown in figure 37.

The secondary interlaminar fractures of the zero-degree tape layers within the skin section were examined on specimens LA1c and LA3d. Those fractures passed through specimen LA1c and all of the specimens from LA3, so that upon cutting, they separated into three layers, with the middle layer being the zero-degree tape with interlaminar fractures on each side. The outside piece of LA1c was used to examine the outboard surface of the outboard fracture, and the inboard piece of LA3d was used to investigate the inboard surface of the inboard fracture. In both cases, the surfaces were fabric with tape fibers and imprints overlaid. On both specimens, the hackles that were observed all pointed upward along the zero-degree fibers parallel to the stringers.

Specimens LA5 and LA7a from the skin section included interlaminar fracture surfaces both on the inboard and outboard sides of the specimens, where the skin layers separated from the precured lug layers. For both specimens, the outboard surface was a zero-degree/90-degree weave with –45-degree fabric imprints overlaid. In general, hackles were observed pointing mainly forward, perpendicular to the stringer structure. There were some hackles pointing in opposite directions on adjacent bundles, and a pattern where hackles pointed inward toward the crossing bundle. The crack propagation direction appeared to be generally aft where it could be determined.

Specimens LA6 and LA8 were cut from the stringer module structure at the lower end of the upper piece (figure 30). The surfaces of these two specimens had identical morphology, with tape fibers and imprints from the stringer outer flange layers over +45-degree fabric, and the fracture features observed were also similar. In general, the hackles that were observed pointed upward parallel to the stringer structures. The crack propagation directions were generally to the aft and upward, except in specimen LA8e, where the crack propagation direction was more forward and upward.

Microscopic matrix porosity was observed in many localized areas throughout the interlaminar fracture surfaces in the vicinity of the left aft lug, generally associated with the brown deposits visible in the corners where the bundles in the fabric cross one another. Examples are shown in figures 38 and 39. Figure 39 also shows a surface morphology that was not uncommon, with relatively ill-defined hackles. In addition to the microscopic matrix porosity, there were also areas where the matrix had a granular appearance, which was often accompanied by fiber fragments. Matrix granularity was common in specimens LA6 and LA8, but was also observed in other areas. An example from the outer piece of specimen LA1c is shown in figure 40.

3.5. Left Center

An overall view of the left center lug area fracture is shown in figure 41. A translaminar fracture occurred in the vertical stabilizer structure above the lug bore at the rib 1 fastener row as shown in figure 41, intersecting most of the rib 1 fastener holes. The fracture was horizontal and perpendicular to the skin surface. As shown in figure 42, the fracture surfaces generally appeared rough, consistent with fracture primarily under tensile loading.

Two specimens, labeled LC1 and LC2 in figure 41 and containing areas of the translaminar fracture surface, were cut from the lower piece. As cutting was completed, specimen LC1 split into four pieces, and specimen LC2 split into 3 pieces. From inboard to outboard and as measured near the center and adjacent to the translaminar fracture surface, the thickness of each piece was 0.08, 0.85, 0.60, and 0.11 inches for specimen LC1 and 0.031, 0.50, and 0.41 inches for specimen LC2. Some dimples and arc-shaped scratches were observed on the disbonded interlaminar surfaces between the thickest pieces of both of these specimens. Typical features observed for the outboard surface between the thickest pieces of LC2 are shown in figure 43.

The translaminar fracture surfaces on specimens LC1 and LC2 were examined using SEM. The fracture features for these specimens were similar. For fibers oriented in the zero degree direction, the fibers near the center of the thickness and near the inboard surface showed radial fracture patterns over their fracture surfaces, consistent with overstress fracture under tensile loads. For the fracture on specimen LC1, the direction of fracture near the center of the thickness was slightly to the left of aft, but near the inboard surface, the general direction of fracture was midway between the right and aft directions. Within approximately 0.2 inch of the outboard surface on both specimens LC2 and LC1, the zero-degree fibers generally had relatively smooth fracture features with changes in the fracture plane within the fibers (called chop marks), features consistent with local fiber bending under compressive load. Typical fracture surface features near the outboard surface for fibers oriented in the zero-degree orientation are shown in figure 44.

3.6. Left Forward

An overall view of the left forward lug translaminar fracture is shown in figure 45 after sectioning from the vertical stabilizer, and a view of the upper fracture surface is shown in figure 46. The lower portion of the lug, which remained with the fuselage, had a darkened appearance consistent with severe exposure to heat and fire.

The translaminar fracture surfaces intersected the lug attach hole. On the aft leg of the lug shown in figure 47, the translaminar fracture was primarily on a horizontal plane and appeared rough, consistent with fracture under tensile loading. On the forward leg of the lug shown in figure 48, the translaminar fracture intersected the bore nearly tangentially and was primarily on a plane parallel to the zero-degree fiber direction. The fracture surfaces on the forward leg of the lug were rough with multiple ply separations in the leg above the fracture surface, consistent with tensile fracture with transverse shear. Views of

the ply separation at the aft and forward surfaces of the lug are shown in figures 49 and 50. On the outboard side of the hole above the bore, a bearing indentation was observed as shown in figure 45. The indentation was approximately 1/8 inch deep and the shape corresponded to the profile of the upper end of the outboard lug on the fuselage clevis attach fitting.

Above the lug fracture, an interlaminar fracture was observed where the stringer module and outer flange layers were separated from the precured lug layers. Rib 1 fasteners at the lower end of the stringer module layers were pulled through the layers. The interlaminar fracture intersected the lower surface of the vertical stabilizer from the front spar aft to approximately 1.5 inches aft of stringer 21. The interlaminar fracture intersected the forward surface of the vertical stabilizer from rib 1 to above rib 2 as shown in figure 51. A visible gap of approximately 5/32 inch was observed at the forward lower end between the inner precured lug structure and the stringer outer flange structure. Above rib 2, another gap of approximately 1/8 inch was also visible between the skin and the stringer outer flange adjacent to the front spar. Ultrasonic C scans performed by NASA and by Airbus indicated a continuous interlaminar separation extending back from the front spar to stringer 22 up to rib 2, and continuing separately along the front spar and stringer 23 up to approximately 2 to 6 inches below rib 3. For more details of the nondestructive examination, see Materials Laboratory Factual Report 02-078.

The left forward lug was cut at the locations shown in figure 45. After cutting, specimen LF3b (from the aft leg of the lug) fell into three pieces, and specimen LF3c (from the forward leg of the lug) split into four pieces. The thickness of each piece was measured adjacent to the cut near the bore (outside of the tapered region where the hat bushing was located). The inboard, center, and outboard pieces of specimen LF3b measured 1.37 inches, 0.16 inches, and 0.13 inches, respectively. The inboard, inboard center, outboard center, and outboard pieces of specimen LF3c measured 0.75 inches, 0.16 inches, 0.44 inches, and 0.24 inches, respectively. For specimen LF3c, the translaminar fractures on the inboard center and the outboard pieces were primarily in a horizontal plane, and for the other two pieces, the fracture plane was primarily parallel to the zero-degree fibers. At the aft end of the inboard center piece of specimen LF3c, the lower ends of the layers were bent to the right.

The translaminar fracture surface on the inboard piece of specimen LF3b (the majority of the aft leg of the lug) was examined using SEM. Fracture features were similar for fibers oriented in the zero degree and 45 degree directions. The fiber fractures typically showed radial fracture patterns over their fracture surfaces, features consistent with overstress fracture under tensile loads. In some areas, particularly near the aft portion of the fracture surface, some of the zero-degree and 45-degree fibers had relatively smooth fracture features with changes in the fracture plane within the fibers (chop marks), features consistent with local fiber bending under compressive load. Figure 52 shows typical fracture features for fibers oriented in the zero degree direction. Unlabeled arrows in figure 52 indicate the direction of fracture for individual fibers. The direction of fracture was sampled from fibers with radial fracture patterns at many locations throughout specimen LF3b, and the general direction of fracture was slightly to the left of aft.

The translaminar fracture surfaces on the outboard and the inboard center pieces of specimen LF3c (pieces from the forward leg of the lug with a horizontal translaminar fracture plane) were examined using SEM. Fracture features were similar for fibers oriented in the zero degree, 45 degree, and 90 degree directions. The fiber fractures typically showed radial fracture patterns over their fracture surfaces, features consistent with overstress fracture under tensile loads. In isolated areas, some of the zero-degree and 45-degree fibers had relatively smooth fracture features with changes in the fracture plane within the fibers (chop marks), features consistent with local fiber bending under compressive load. Figure 53 shows typical fracture features for fibers oriented in the zero degree direction. Unlabeled arrows in figure 53 indicate the direction of fracture for individual fibers. The direction of fracture was sampled from fibers with radial fracture patterns at many locations throughout these two pieces of specimen LF3c. The general direction of fracture was slightly to the left of forward on the inboard center piece, and slightly to the left of aft on the outboard piece.

The interlaminar fracture on the outboard side of the inboard piece of specimen LF3b was examined using SEM. Examination of the surface using the SEM showed evidence of hackles associated with shearing deformation at the fracture surface (Mode II or Mode III fracture). However, no microscopic indications of fatigue were observed, including matrix rollers, widespread abrasion, or striations on exposed fiber surfaces or their imprints.

Matrix porosity was observed on the translaminar and interlaminar fracture surfaces that were examined and will be documented in a separate report.

In order to expose the interlaminar fracture surfaces between the stringer module and outer flange layers above rib 1, three cuts were made using a diamond bandsaw. The mating pieces are shown after cutting in figure 54. The first cut was 19 inches from the top of the part (9 inches below rib 3 and 19 inches above rib 2). The second cut was made approximately 2 inches above rib 2 from the front spar back to just aft of the flange of stringer 23. After making these first two cuts, the lengths of the stringer 23 and front spar flange between those two cuts (pieces LF2a and LF2b, respectively, in figure 54) came free from the rest of the part. The third cut was made just aft of the flange of stringer 23 up from the position of rib 1 to 2 inches above rib 2, where it intersected the second cut. Three ribbons of zero-degree tape, each approximately 1 inch wide, bridged between the two pieces and were snipped with wire cutters to finish separating the piece (piece LF3a in figure 54). One ribbon of tape that bridged the two pieces was along the aft flange of stringer 24, and was cut at a location approximately 8 inches above rib 1. The second ribbon of tape was along the forward flange of stringer 23, and was cut approximately 2 inches below rib 2. The third ribbon of tape was along the aft flange of stringer 23, and was cut approximately 4 inches below rib 2.

The interlaminar fracture between pieces LF3 and LF3a was observed primarily on interfaces between zero-degree tape layers and adjacent fabric layers. The tape layers were four plies making up part of the stringer outer flange. These tape layers began

sequentially in the 2 inches above rib 1 and extended up beyond rib 3 and from the front spar aft beyond stringer 22. The adjacent fabric layers were either the stringer module structure layers at the inboard side of the tape layers or the lug, lug compensation, and skin layers at the outboard side of the tape layers. At the outboard side of the tape layers, the locations of the adjacent fabric layers were as follows: a lug compensation layer covering the lug and extending up to 1.5 inches (37 mm) below rib 2, the innermost lug ply above that up to rib 2, and the innermost skin layer above that. The four zero-degree tape layers from the stringer outer flange generally remained attached to the outer lug/skin part, especially at the lower end near rib 1 and in the regions between the stringers. Farther up, in the areas on top of the stringers, the tape layers remained attached to the inner piece retaining the stringer structure. This transition led to the layers that bridged across the interlaminar fracture (which had to be cut), and to intralaminar fractures (through the layer parallel to the fiber direction) where the main fracture surface shifted from one side of the zero-degree tape layers to the other.

Visually, the fracture surfaces appeared relatively smooth and were mainly confined to the matrix in the interfaces between plies. There were some localized areas where fiber fractures had occurred, leaving fragments of fabric or tape behind. Other markings on the surfaces were imprints of the mating surfaces, indicating the architecture of the mating plies and the locations of ply drops. Bundles of aramid fiber used as tracers to indicate the orientation of the fabric plies could also be seen. Over much of the surface, deposits (light tan or dark brown) were observed in the pockets formed where bundles in the woven fabric crossed one another or in regions where plies ended. These deposits appear to be more common higher up the part. No visible indications of crack-arrest marks or patterns that would be associated with fatigue or other long-term pre-existing damage were observed.

Several specimens were cut from the inner part containing the stringer structure labeled piece LF3a (as shown in figure 55) for microscopic examination of the fracture surfaces in the SEM. The specimens (LF3a-1, LF3a-2 and LF3a-3) at the top of piece LF3a straddled the position of rib 2. Specimens LF3a-1a and LF3a-1b were cut apart directly through the rib 2 web. Specimens LF3a-2a and LF3a-2b also straddled the web of stringer 24, which ran up from rib 1 but ended at rib 2. Two specimens were also cut from the top and bottom of piece LF2a (part of stringer 23), and a specimen was cut from the fracture surface at the top of piece LF2b (part of the front spar flange). Each specimen was cut into a piece approximately 2 inches on a side using the diamond bandsaw and/or a low-amplitude vibrating saw with the diamond-edged blade.

In cutting the specimens for examination, additional interlaminar fractures were observed at the midplanes of the webs and outer flanges of stringers 23 and 24. (These interlaminar fractures were perpendicular to the plane of the main interlaminar fracture under investigation.) These fractures did not penetrate through the stringer inner flanges. The interlaminar fractures in the stringers were visible at the base of stringers 23 and 24 where they run out near rib 1. The interlaminar fracture in the web of stringer 24 was not visible at the top part of piece LF3a, and that stringer did not extend up beyond rib 2. The interlaminar fracture in stringer 23 appeared to extend up about 6 inches above rib 2, and when a specimen was cut from the lower end of piece LF2a, it fractured into two pieces.

Another intralaminar fracture (through the tape layers parallel to the fiber direction) was present along the aft edge of the stringer inner flange in these specimens.

For SEM observation, all of the fracture surfaces were sputter coated with a layer of gold/palladium. All but one of the specimens (specimen LF3a-5b from the main interlaminar fracture on piece LF3a, shown in figure 56) were cleaned in deionized water in an ultrasonic cleaner.

Typical views of the fracture surface on specimens from piece LF3a are shown in figures 57 to 60. Examination of the surface using SEM showed evidence of river marks associated with tension across the fractures surface (Mode I fracture) and hackles associated with shearing deformation at the fracture surface (Mode II or Mode III fracture). The hackle features observed were generally sharp and distinct. The SEM examination did not reveal any microscopic indications of fatigue, such as matrix rollers, widespread abrasion, or striations on exposed fiber surfaces or their imprints. An example photograph from the SEM examination of the specimen LF3a-5b (not cleaned) is shown in figure 57. The figure shows the presence of hackles pointing generally upward and forward between the main fibers in the weave, with river marks (also upward and forward) in the matrix pocket formed where the bundles cross. Also indicated is a region of microscopic matrix porosity, which is common.

A number of surface layer and fiber imprint orientations were observed on specimens from piece LF3a. The surfaces of specimens LF3a-2, LF3a-3, LF3a-5, LF3a-7, and LF3a-10 were +45-degree fabric with zero-degree tape fiber imprints. Portions of specimens LF3a-2 and LF3a-3 were zero-degree tape with –45-degree fabric fiber imprints. The surface of specimen LF3a-9 was –45-degree fabric of the rib 1 flange with zero-degree tape fiber imprints. Specimen LF3a-6a was zero-degree tape with faint 45-degree fabric imprints. Specimen LF3a-8 was zero-degree tape fractured on both sides having 45-degree fabric fiber imprints on the outboard surface and –45-degree fabric fiber imprints on the inboard surface. Specimen LF3a-1 was zero-degree tape over +45-degree fabric with areas of –45-degree fabric from the forward spar flange. Specimen LF3a-2 was zero-degree tape over 45-degree fabric with –45-degree fabric fiber imprints.

In general, the hackles throughout the surface of piece LF3a pointed upward parallel to the zero-degree fiber direction along the stringers, and the general crack propagation direction as determined from the river markings was also upward parallel to the zero-degree fiber direction. The exceptions were specimen LF3a-9, which had hackles pointing in all directions and a crack propagation direction downward parallel to the zero-degree direction. In specimen LF3a-6a, the crack propagation direction was not clear. The lower forward area of specimen LF3a-10 had hackles that pointed in the forward and downward direction. The inboard surface of specimen LF3a-8 had hackles pointing in the aft direction perpendicular to the zero-degree fiber direction, and the outboard surface had a crack propagation direction in the aft and downward direction. Specimens from the lower portion of piece LF3a had a crack propagation direction in the downward and forward directions, and the lower aft portion of the specimen from piece LF2b had a crack propagation direction in the downward direction. The surfaces and the general fracture features

observed were also affected by local structures, such as the presence of stringers or the edges of plies.

Piece LF2a was basically stringer 23. Specimen LF2a-1 was taken from the upper end and specimen LF2a-2 was taken from the lower end. The surfaces of these specimens were zero-degree tape layers making up the stringer outer flange, with imprints of -45-degree fabric fibers. Hackles were observed pointing in all directions, but the crack propagation direction was generally upward.

The surface layer of specimen LF2b-1, cut from the upper end of piece LF2b (figure 54), also was zero-degree tape making up the stringer outer flange, with imprints of –45-degree fabric fibers. This specimen was part of the front spar flange, almost directly above the position of stringer 24, and the tape layers from that area continued up to this point. Hackles were observed pointing in all directions. The crack propagation direction was generally upward and toward the aft with respect to the zero-degree fiber direction, which was shown by river marks in matrix pockets and also by the faint bands[5] seen in figure 61.

Matthew R. Fox
Materials Engineer

Carl R. Schultheisz
Materials Research Engineer

[5] Although similar in appearance to the crack arrest marks seen in the fatigue of metals, these features are not associated with fatigue in composites. These marks do indicate the crack propagation direction, from the concave to the convex side of the marks.

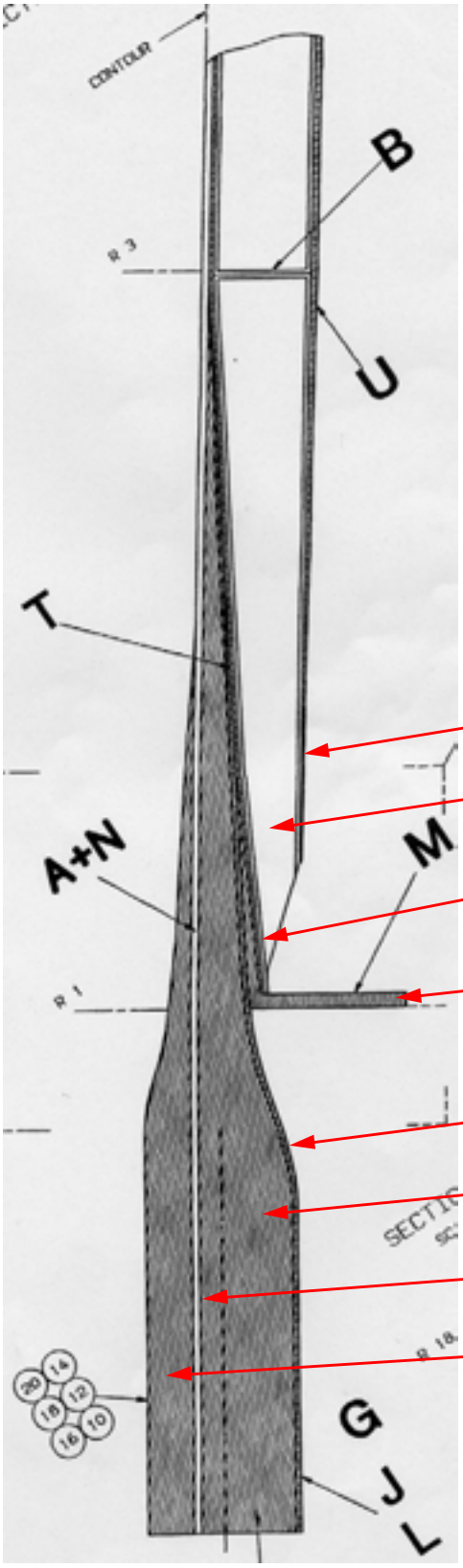

ImageNo:210A0048, Project No:A00387

Figure 1. Engineering drawing of a typical lug cross section in the plane parallel to the zero-degree fiber direction.

ImageNo:210A0047, Project No:A00387

Figure 2. Overall view of the right aft lug viewed from the right showing the upper fracture surfaces. As recovered, a piece of rib 1 was displaced over a portion of the fracture surface.

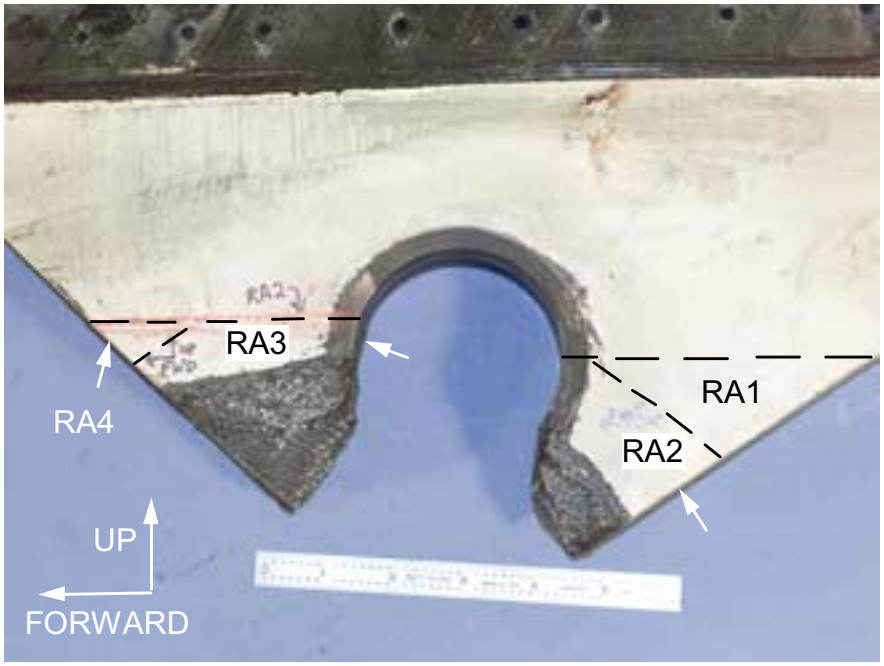

ImageNo: 210A0035, Project No:A00387

Figure 3. View of the right aft lug looking from the left. Dashed lines indicate where cuts were made.

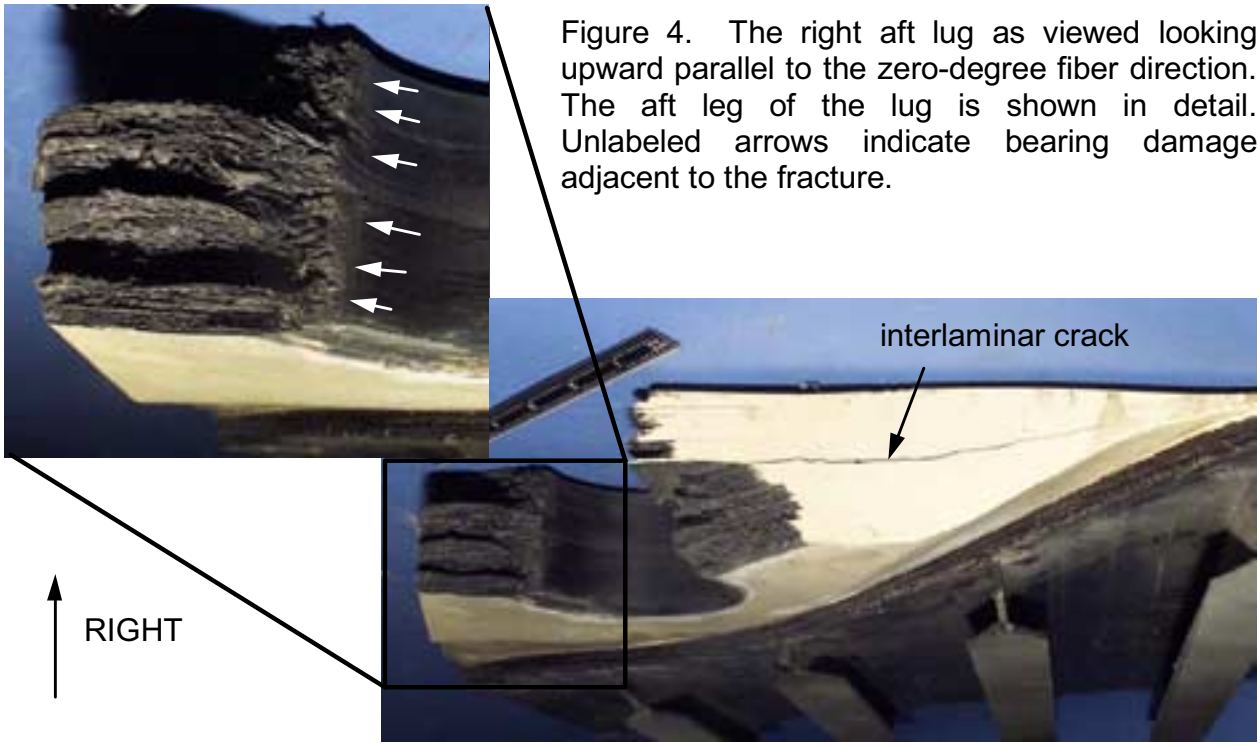

Figure 4. The right aft lug as viewed looking upward parallel to the zero-degree fiber direction. The aft leg of the lug is shown in detail. Unlabeled arrows indicate bearing damage adjacent to the fracture.

ImageNo:210A0039, Project No:A00387

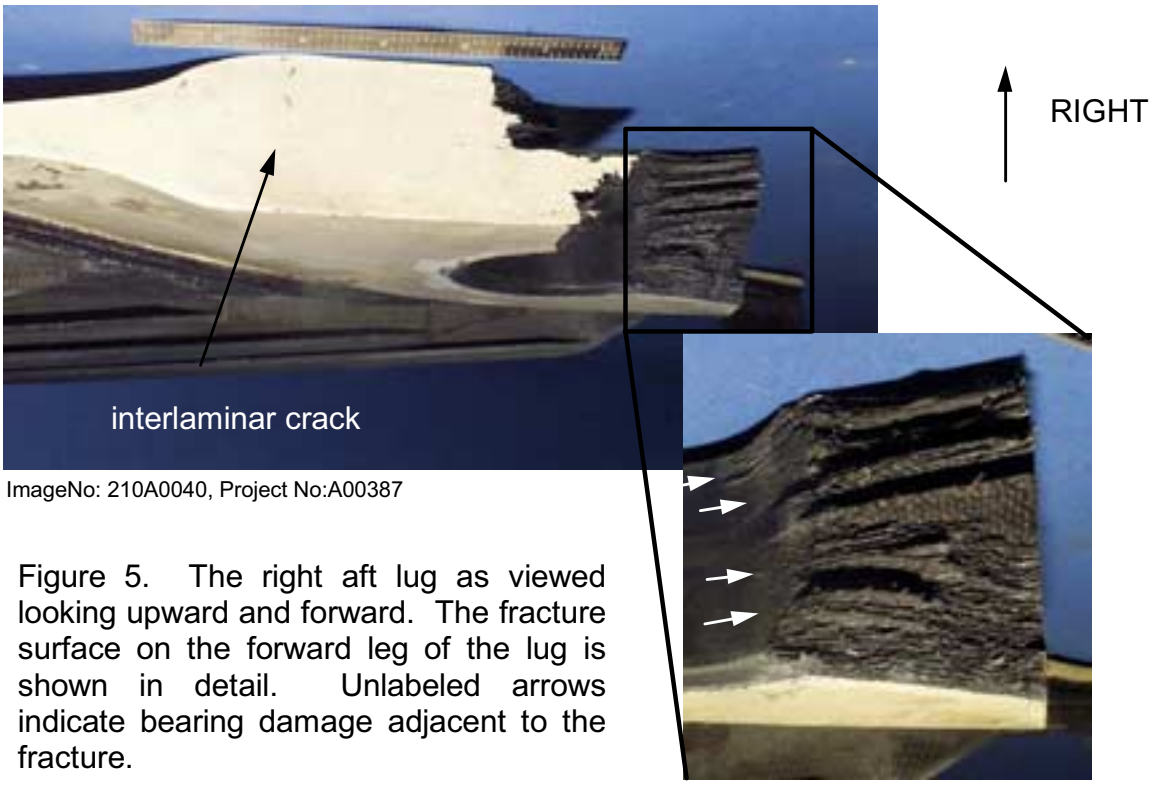

ImageNo: 210A0040, Project No:A00387

Figure 5. The right aft lug as viewed looking upward and forward. The fracture surface on the forward leg of the lug is shown in detail. Unlabeled arrows indicate bearing damage adjacent to the fracture.

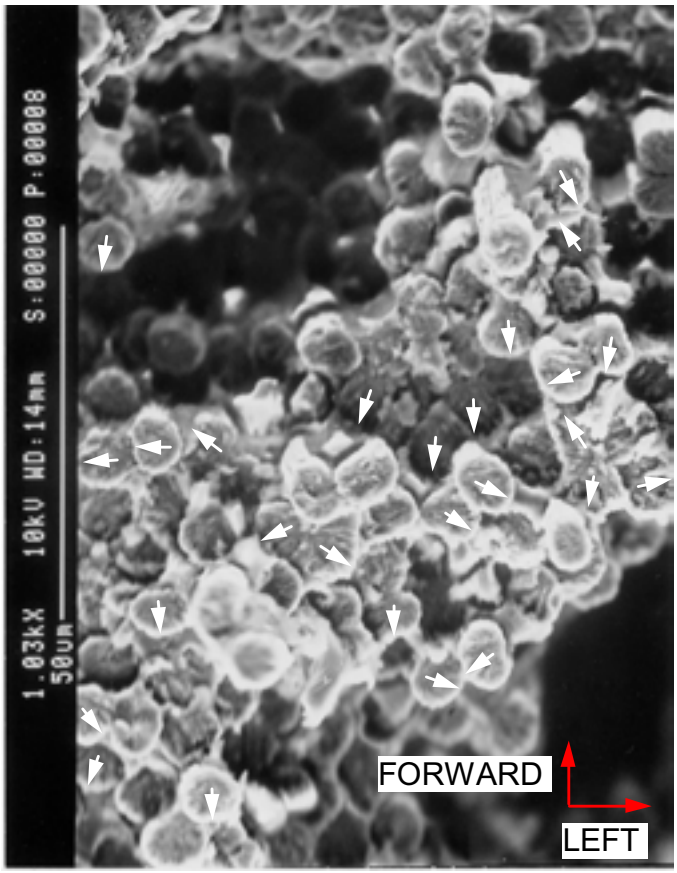

Figure 6. Typical appearance of the fractured zero-degree fibers on specimen RA2-1 near the outboard surface. Arrows on fractured fibers indicate direction of fracture propagation through the fiber.

Figure 7. Typical appearance of the fractured -45-degree fibers on specimen RA2-1 near the center of the total lug thickness. Arrows on fractured fibers indicate direction of fracture propagation through the fiber.

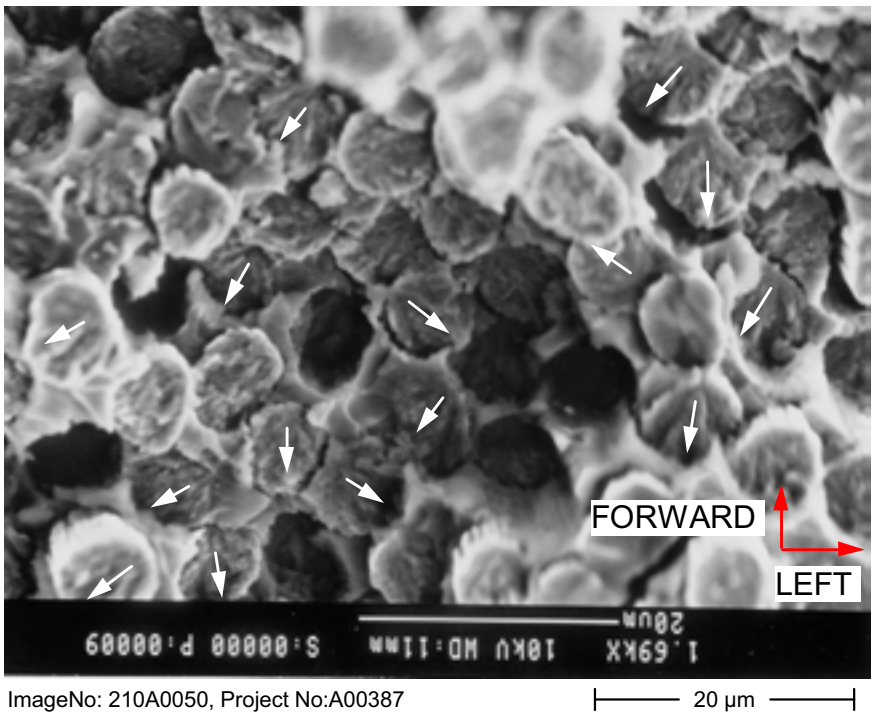

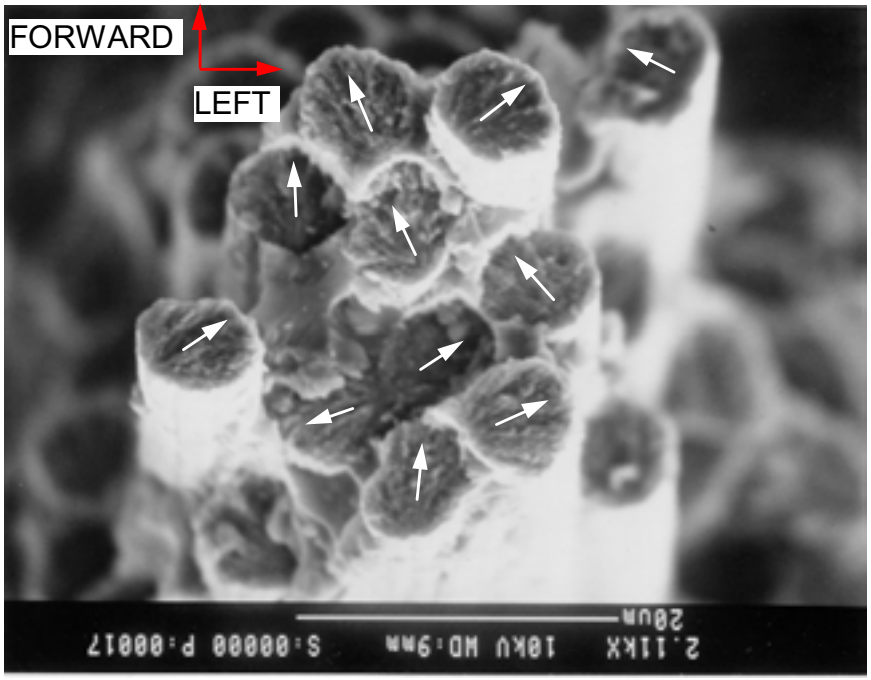

Figure 8. Typical appearance of the fractured zero-degree fibers on specimen RA3-2 near the center of the total lug thickness. Arrows on fractured fibers indicate direction of fracture propagation through the fiber.

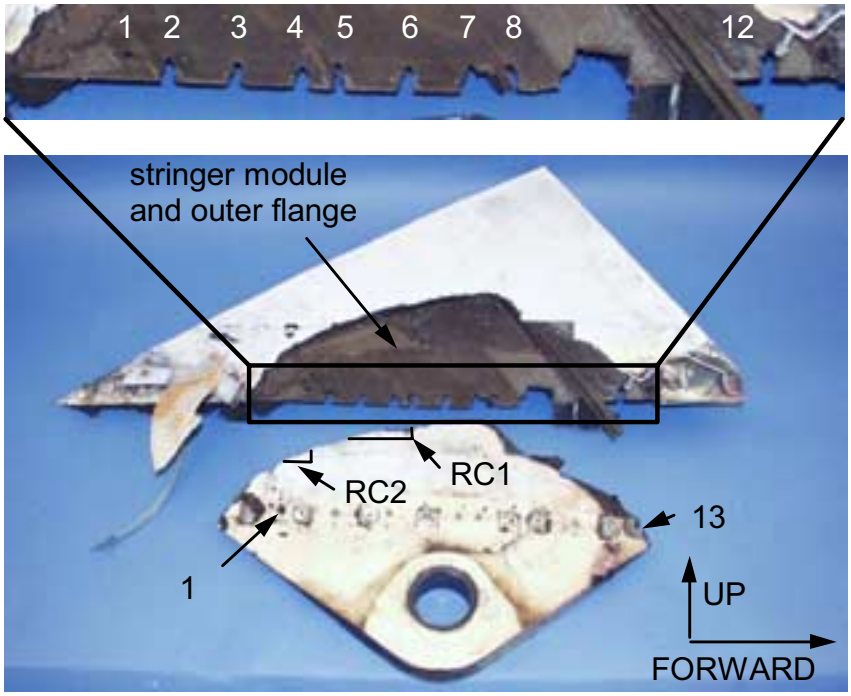

ImageNo:209A0282, Project No:A00387

Figure 9. Overall view of the right center lug pieces viewed from the right with the upper photograph showing details of the rib 1 fastener hole tearouts in the stringer module and outer flange layers.

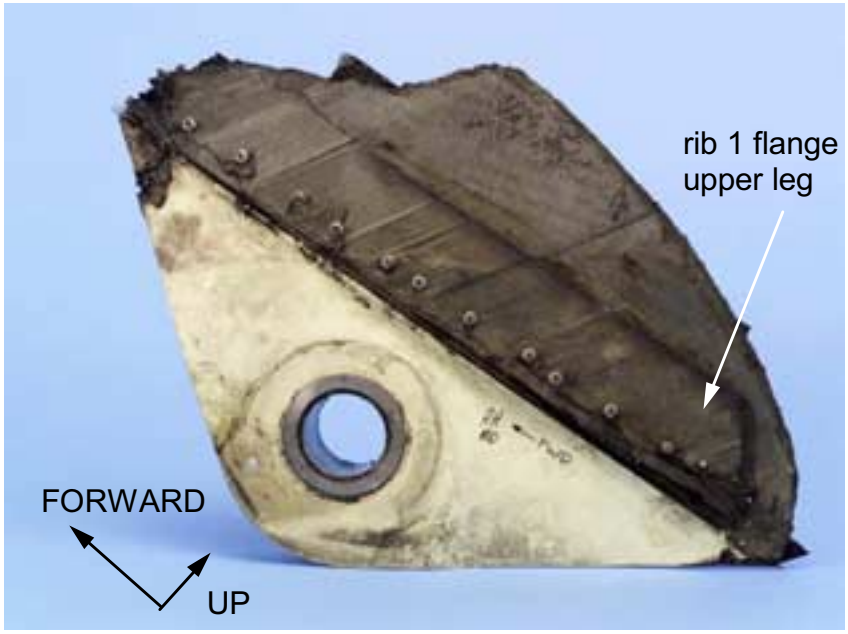

ImageNo: @ImageNo/2@, Project No:A00387

Figure 10. Overall view of the right center lug, lower piece, looking from the left.

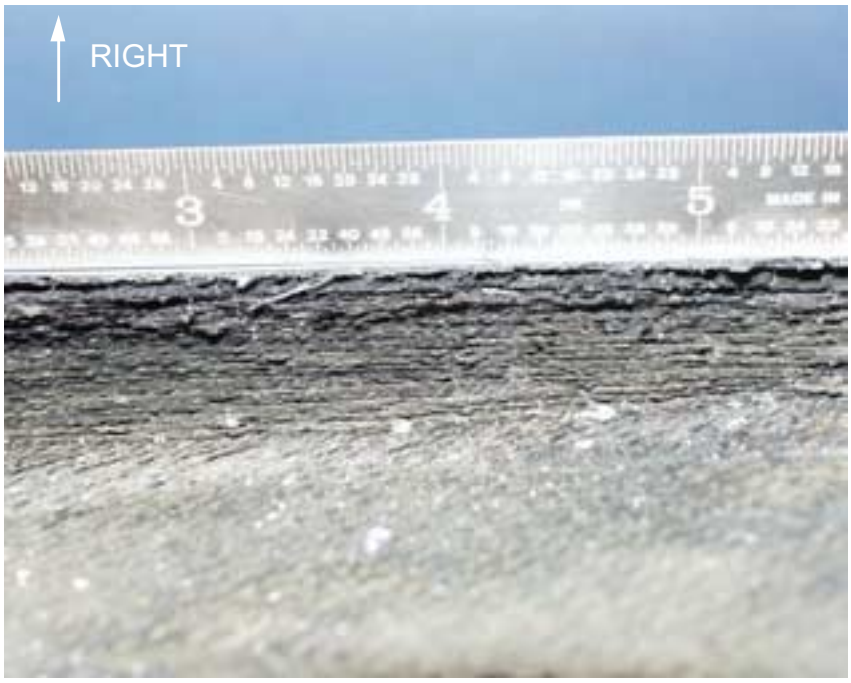

ImageNo:209A0307, Project No:A00387

Figure 11. Right center lug upper fracture surface viewed looking upward parallel to the zero-degree fiber direction.

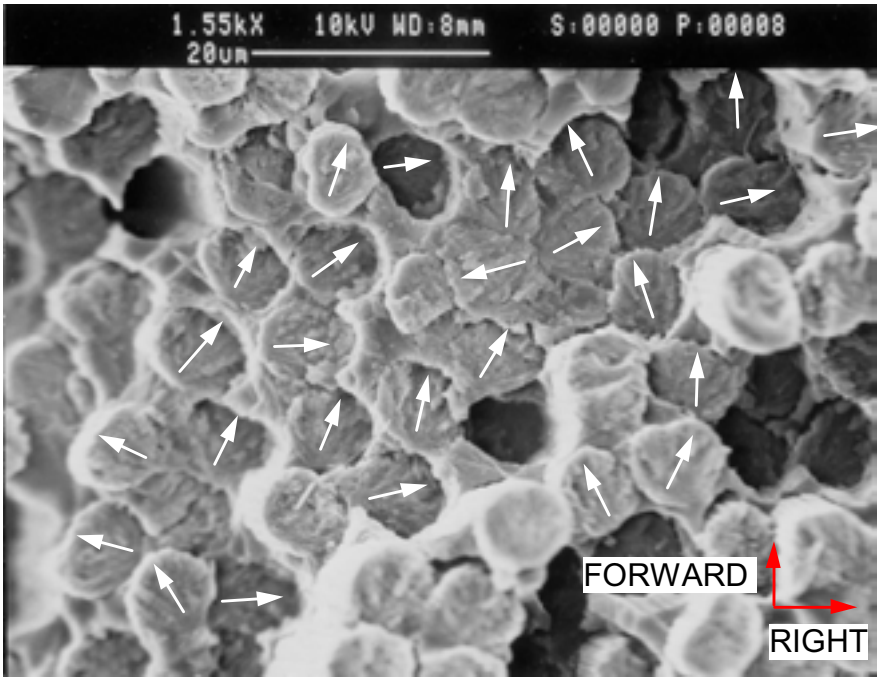

ImageNo:209A0123, Project No:A00387 20 µm

Figure 12. Typical appearance of the fractured zero-degree fibers on spedimen RC2 near the exterior surface. Arrows on fractured fibers indicate direction of fracture propagation through the fiber.

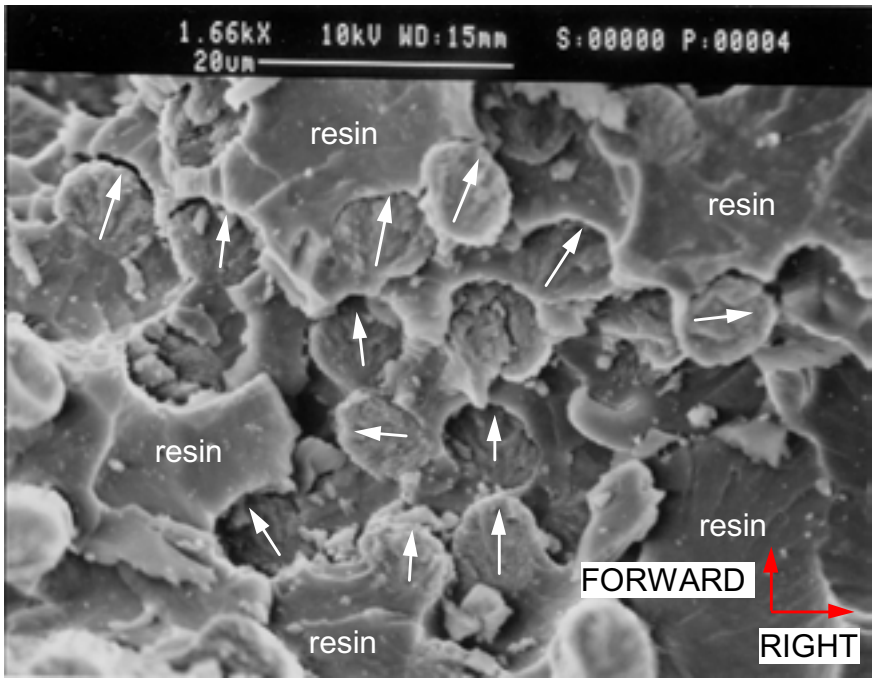

Figure 13. Typical appearance of the fractured zero-degree fibers on sample RC1 near the exterior surface. Arrows on fractured fibers indicate direction of fracture propagation through the fiber.

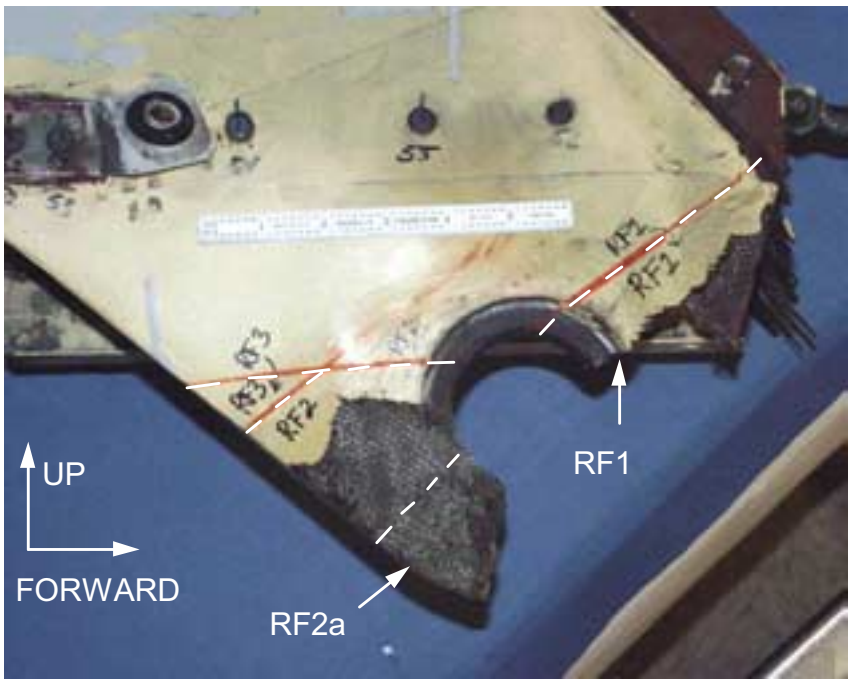

Figure 14. Overall view of the right forward lug upper fracture area. Dashed lines indicate locations where cuts were made.

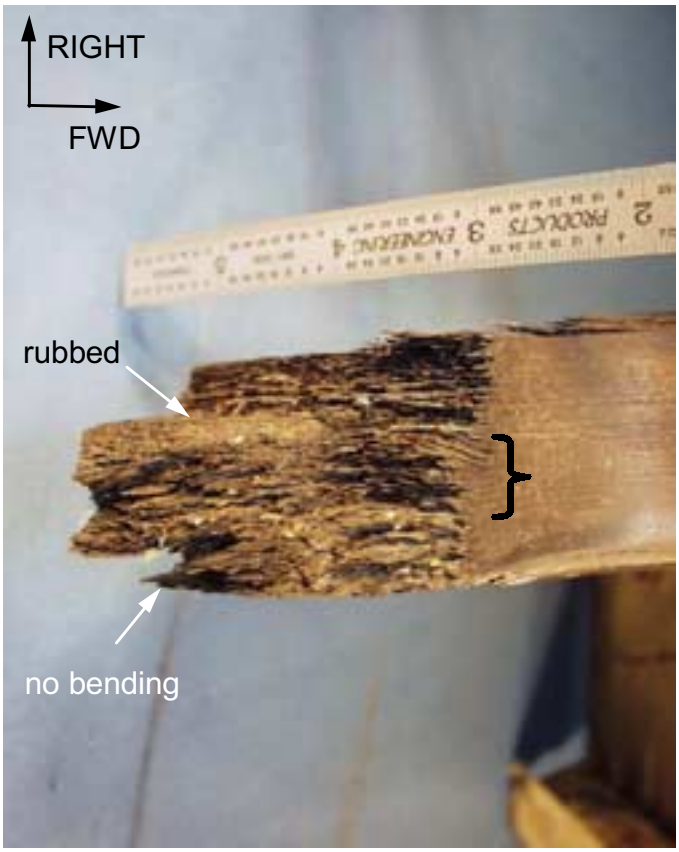

ImageNo:209A0419, Project No:A00387

Figure 15. Direct view of the right forward lug, aft leg looking upward and aft. The bracket indicates fiber ends bent to the right.

Figure 16. The aft surface of the right forward lug above the fracture through the aft leg, showing delaminations. View is looking upward and forward. The bracket indicates fiber ends bent to the left.

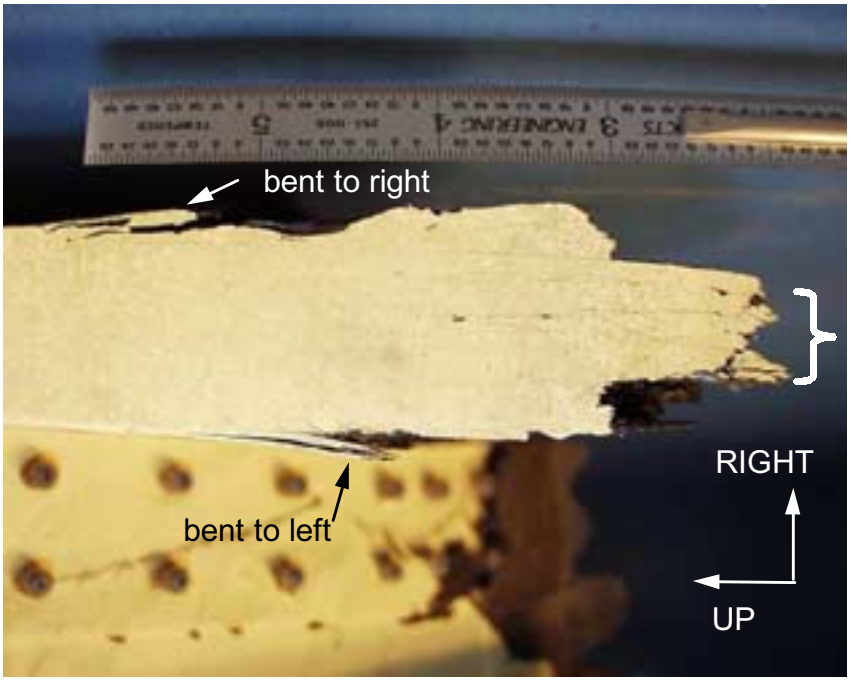

ImageNo: 209A0418, Project No:A00387

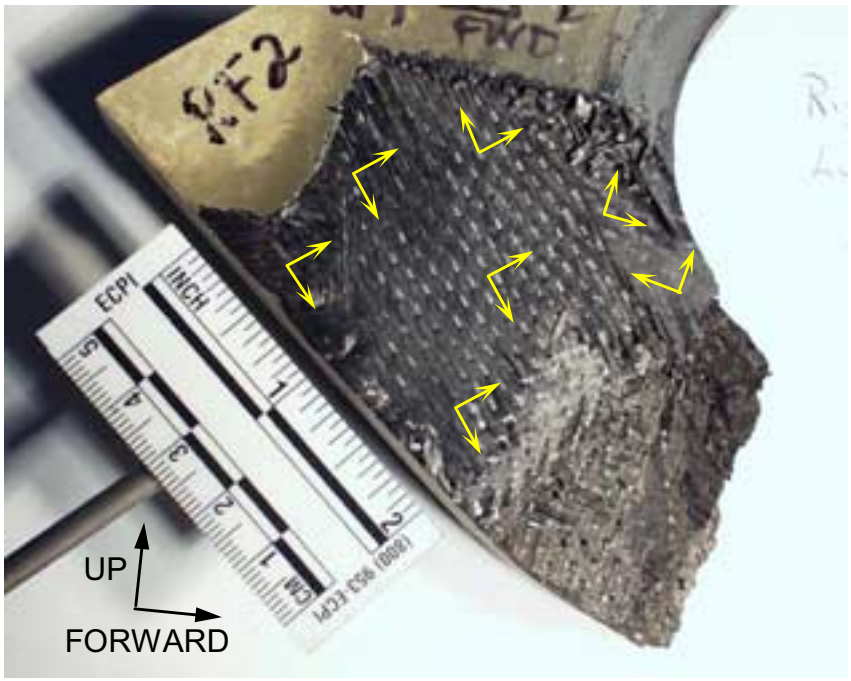

ImageNo:209A0440, Project No:A00387

Figure 17. Aft leg of the right forward lug showing the outer delamination surface. Arrows indicate directions of hackles observed. Shear tractions on the surface acted opposite to the direction of the hackles.

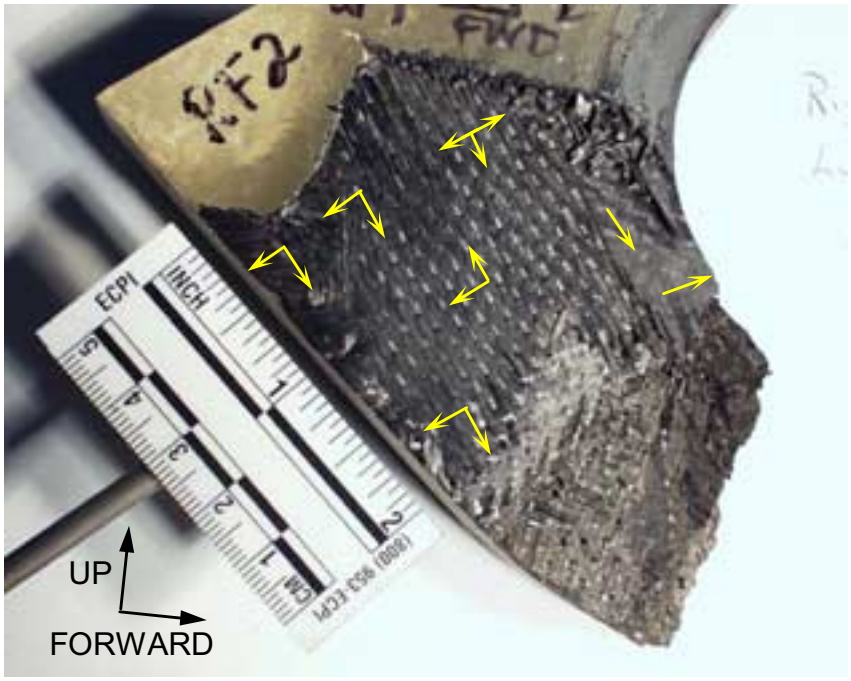

ImageNo: 209A0440, Project No:A00387

Figure 18. Aft leg of the right forward lug showing the outer delamination surface. Arrows indicate the direction of the river markings at the bases of the hackles.

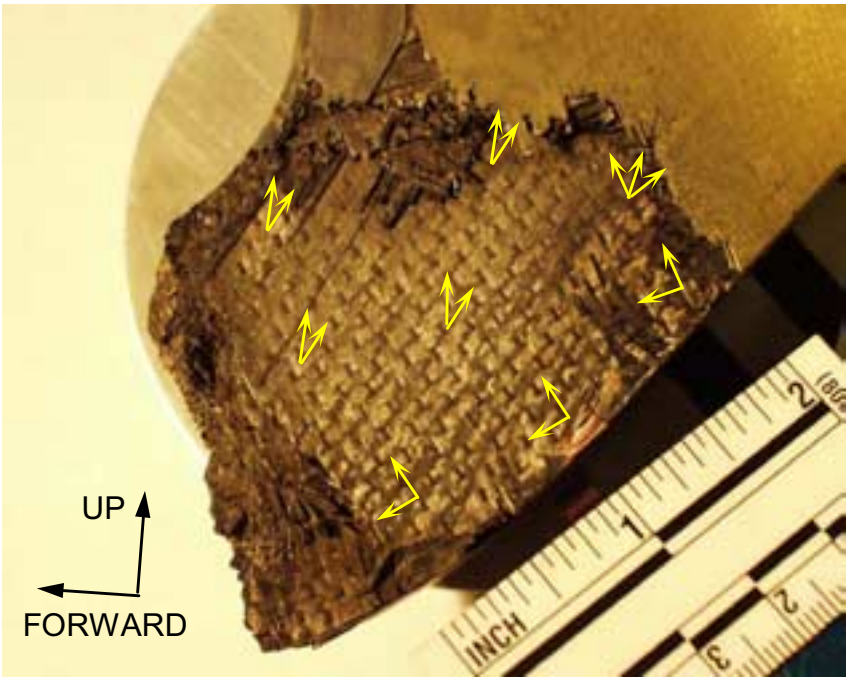

ImageNo:209A0441, Project No:A00387

Figure 19. Aft leg of the right forward lug showing the inner delamination surface. Arrows indicate directions of hackles observed. Shear tractions on the surface acted opposite to the direction of the hackles.

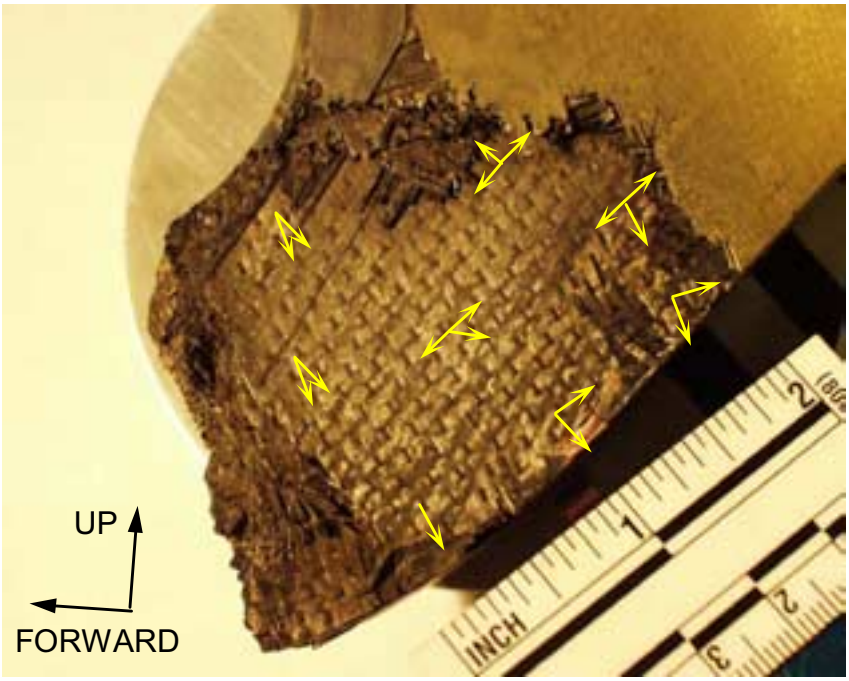

ImageNo: 209A0441, Project No:A00387

Figure 20. Aft leg of the right forward lug showing the inner delamination surface. Arrows indicate the direction of the river markings at the bases of the hackles.

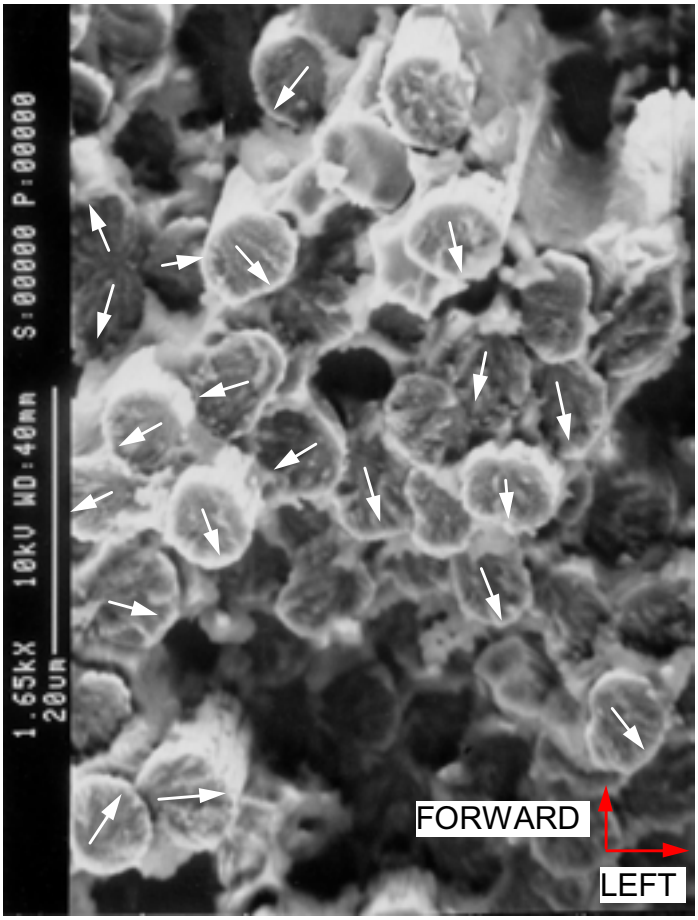

Figure 21. Typical appearance of the fractured zero-degree fibers on sample RF2a near the exterior surface. Arrows on fractured fibers indicate direction of fracture propagation through the fiber.

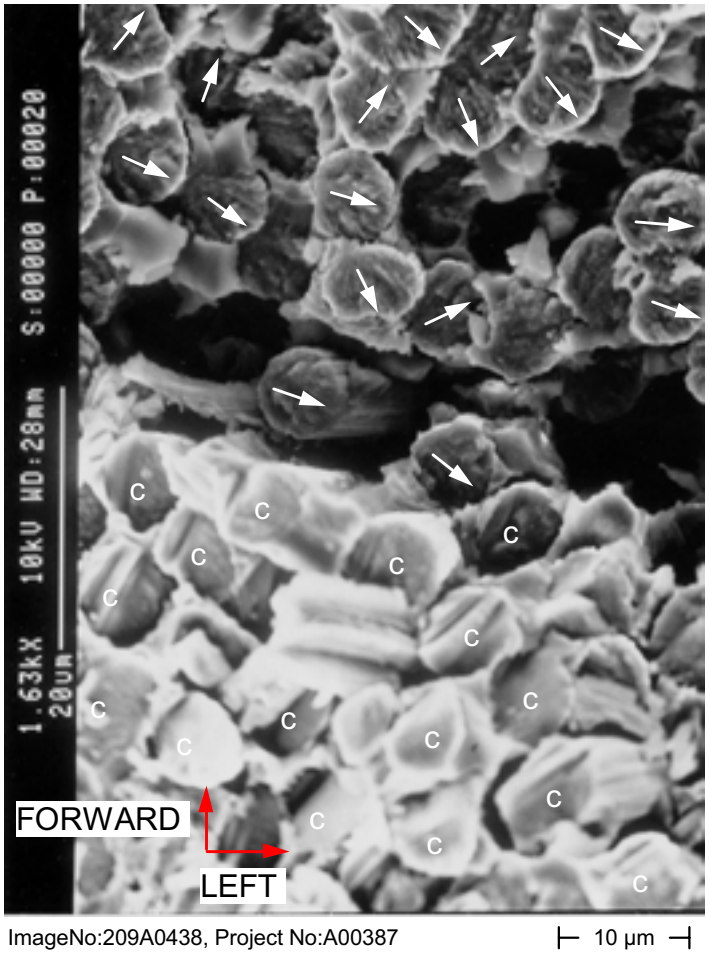

Figure 22. Typical appearance of the fractured zero-degree fibers on sample RF2a near the forward and center portions of the fracture. Arrows on fractured fibers indicate direction of fracture propagation through the fiber. Arrows "c" indicate fiber ends having chop marks.

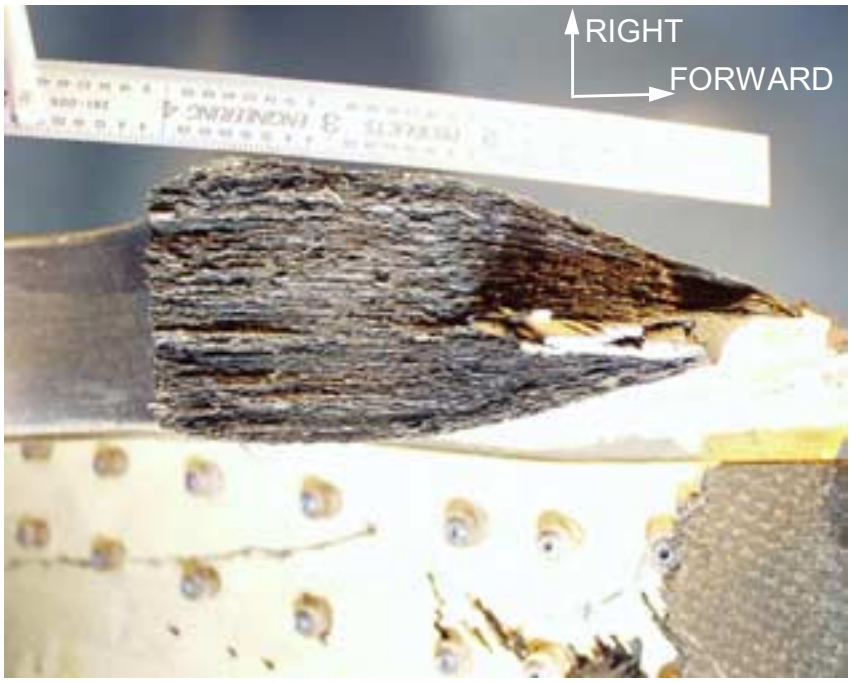

ImageNo:209A0416, Project No:A00387

Figure 23. Fracture surface on the forward leg of the right forward lug, View is looking upward parallel to the zero-degree fiber direction.

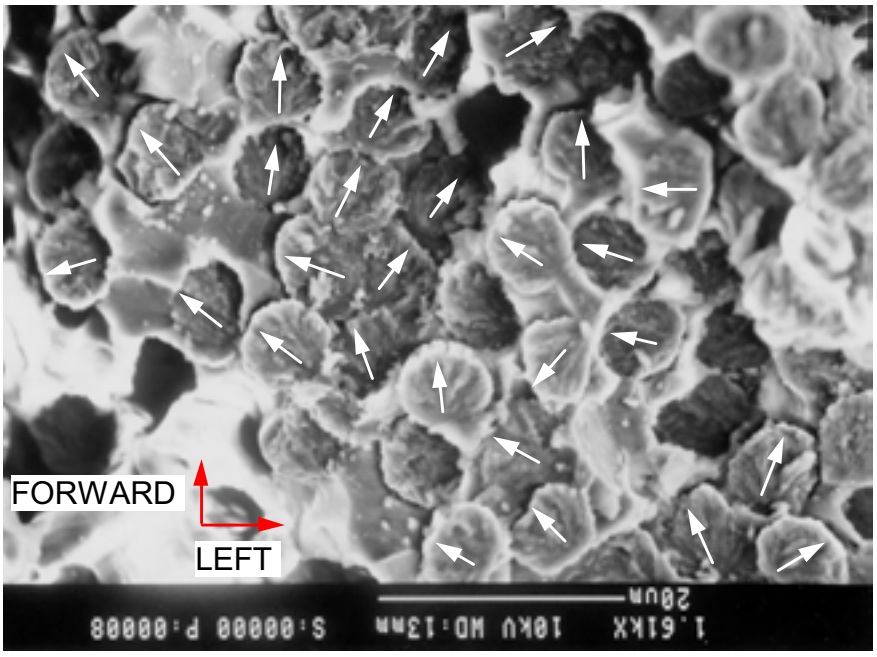

ImageNo:209A0436, Project No:A00387 — 20 µm

Figure 24. Typical appearance of the fractured zero-degree fibers on sample RF1 near the outer and aft portions of the fracture. Arrows on fractured fibers indicate direction of fracture propagation through the fiber.

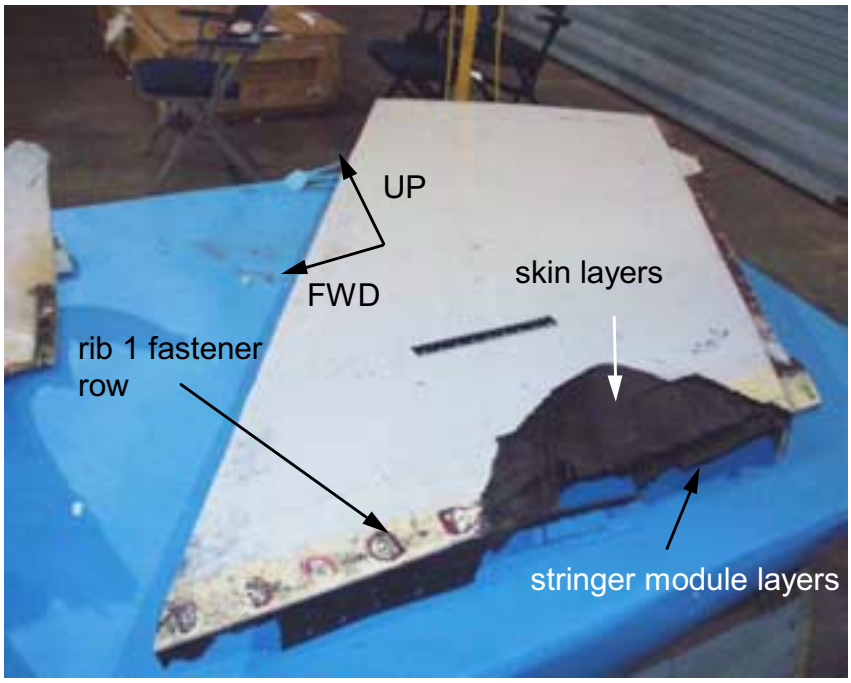

ImageNo:209A0398, Project No:A00387

Figure 25. Overall view of the upper piece containing the upper portion of the fracture at the left aft lug, viewed looking up and to the right.

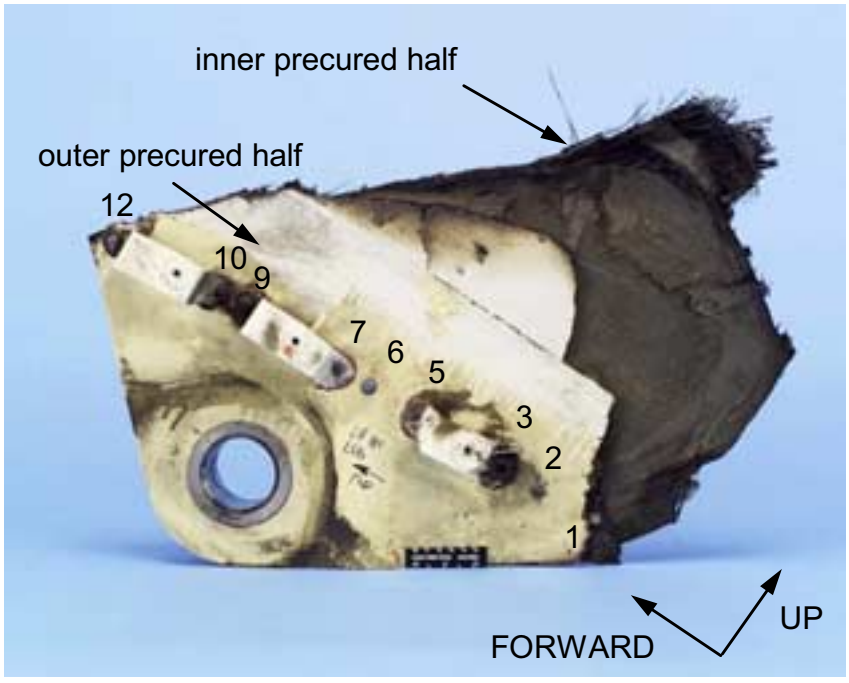

ImageNo: 209A0395, Project No:A00387

Figure 26. Overall view of the lower piece containing the lower portion of the fracture at the left aft lug, viewed looking to the right.

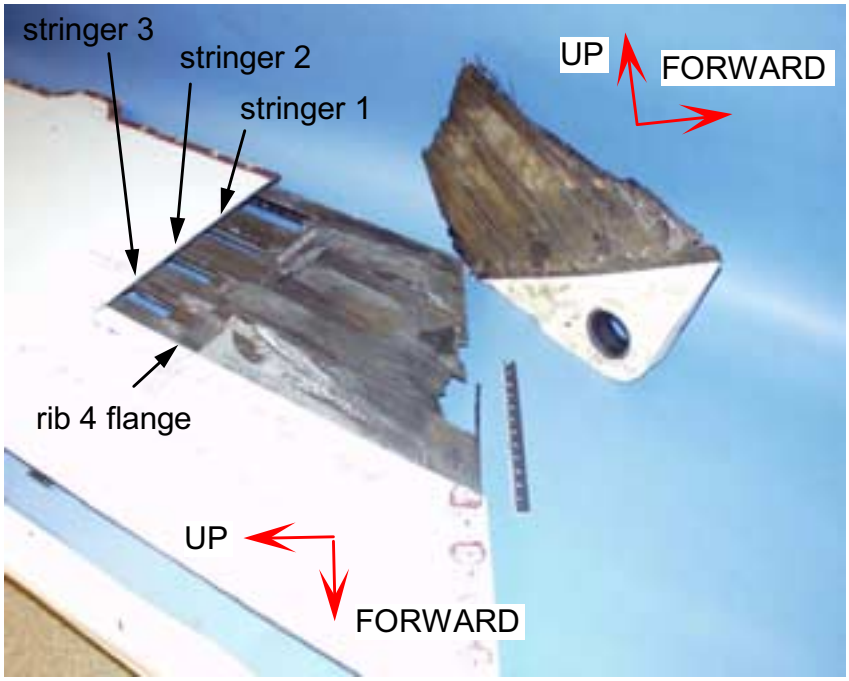

ImageNo: 209A0283, Project No:A00387

Figure 27. Mating fracture surfaces at the left aft lug area between the lower piece and the stringer module structure of the upper piece after cutting through the skin.

ImageNo:210A0003, Project No:A00415

Figure 28. Inner surface of the vertical stabilizer skin section at the left aft lug after cutting from the upper piece. The lower portion of this interlaminar surface mates to the outer surface of the inner precured lug half.

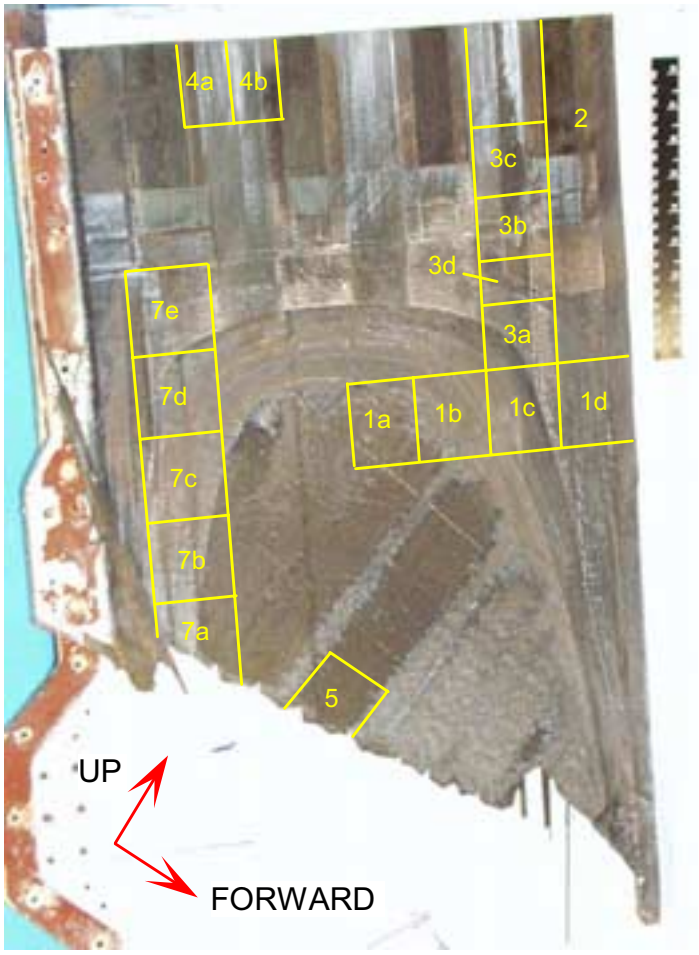

ImageNo:210A0003, Project No:A00415

Figure 29. Specimens cut from the skin section at the left aft lug fracture area for examination using SEM.

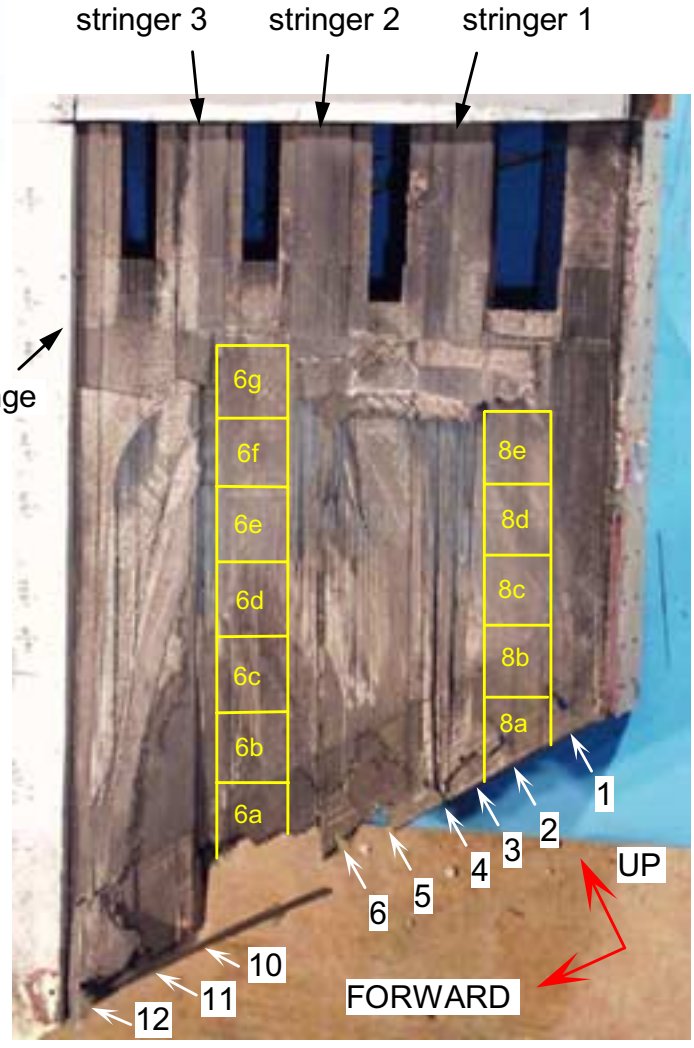

ImageNo: 210A0004, Project No:A00415

Figure 30. Specimens cut from the stringer module structure of the upper piece for examination using SEM. Rib 1 fastener holes are numbered at the bottom of the part.

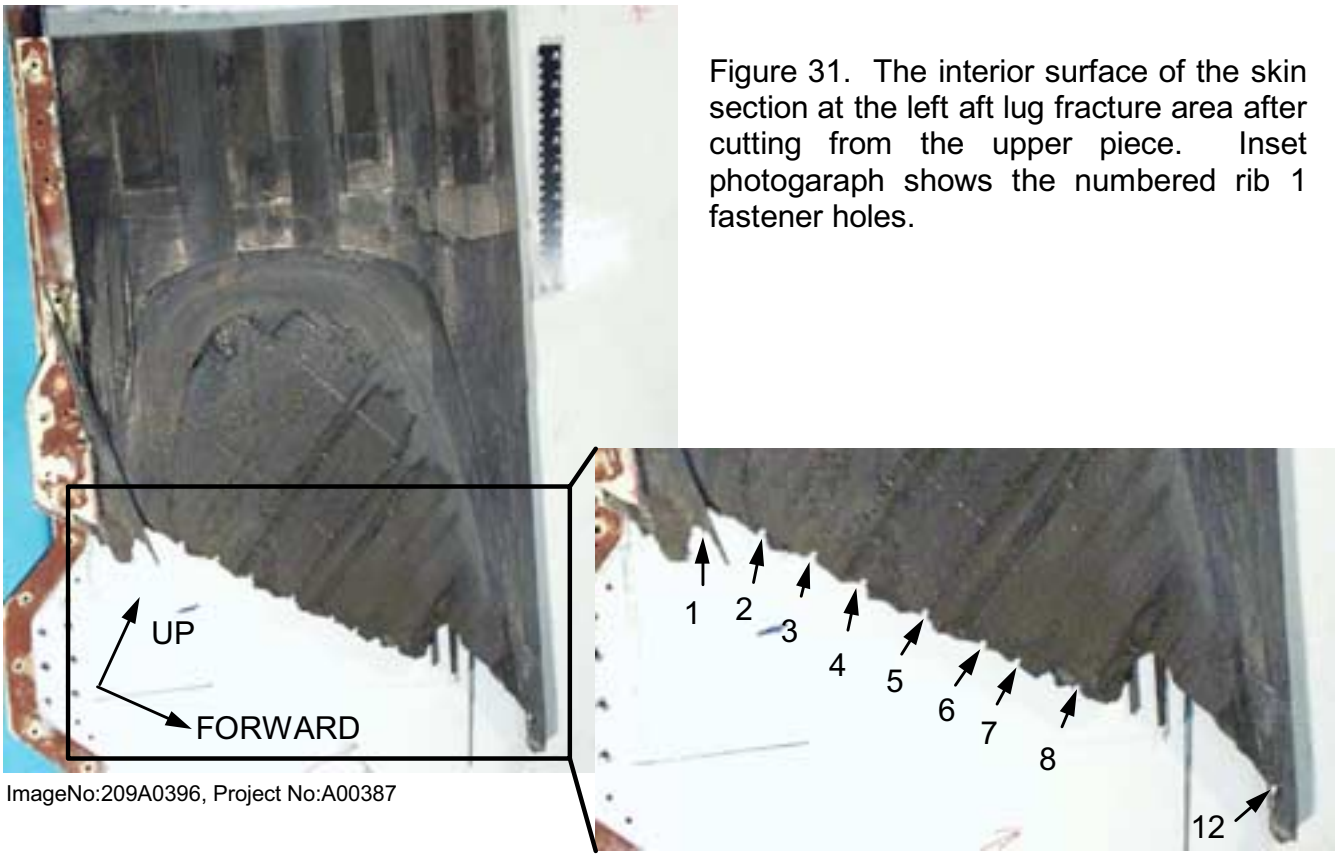

ImageNo:209A0396, Project No:A00387

Figure 31. The interior surface of the skin section at the left aft lug fracture area after cutting from the upper piece. Inset photogaraph shows the numbered rib 1 fastener holes.

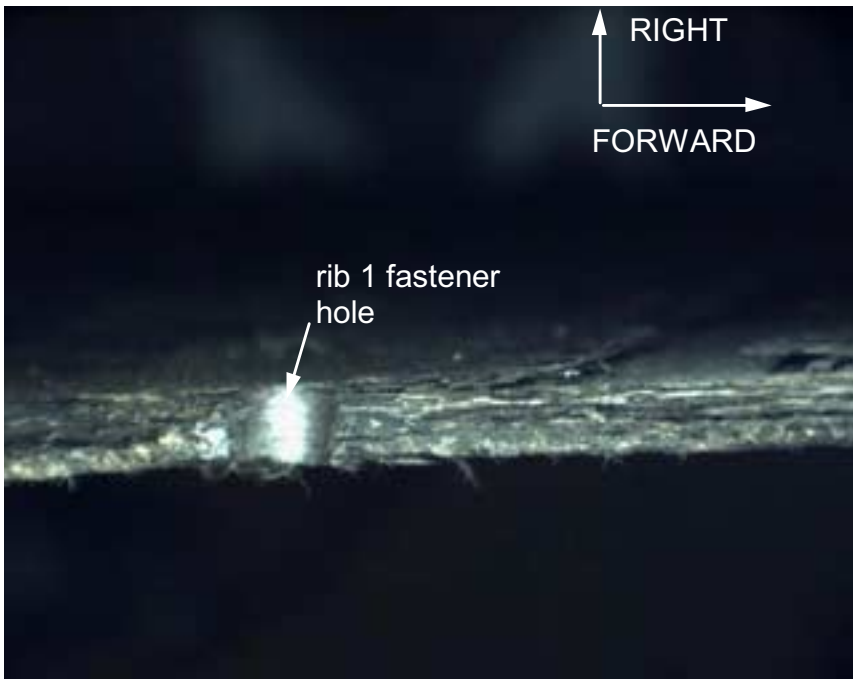

ImageNo:209A0403, Project No:A00387 — 10 mm

Figure 32. Vertical stabilizer skin fracture at a rib 1 fastener hole in the vicinity of the left aft lug, viewed looking upward.

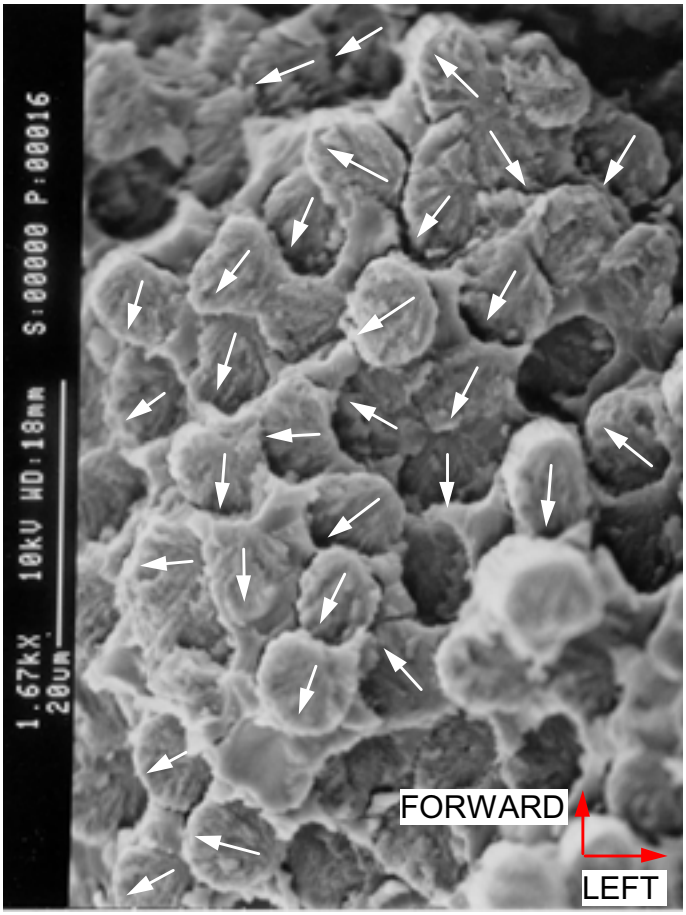

Figure 33. SEM photograph with arrows indicating the direction of tensile crack propagation on the ends of zero-degree fibers from the inside edge of specimen LA5a.

Figure 34. SEM photograph from the center of specimen LA5a. Arrows indicate the direction of tensile crack propagation and labels "c" indicate compressive failure on the ends of zero-degree fibers.

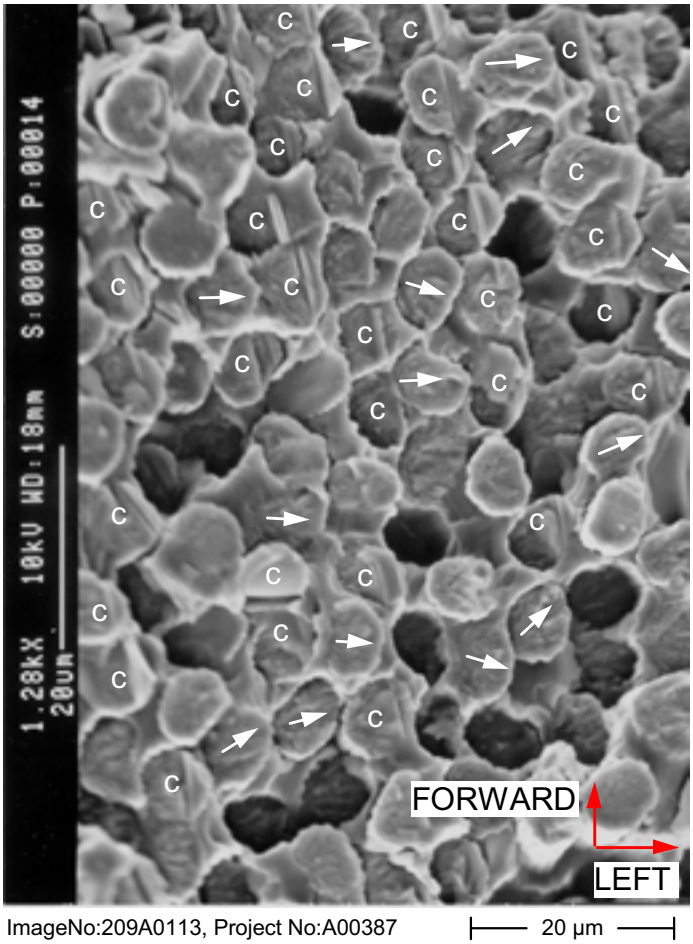

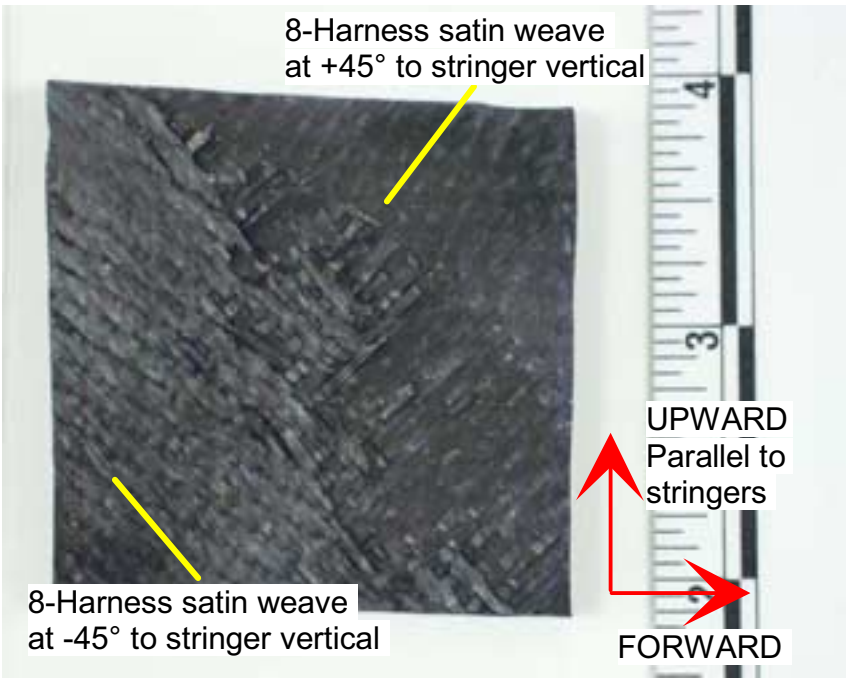

ImageNo:208A0426, Project No:A00415

Figure 35. Fracture surface of specimen LA1a.

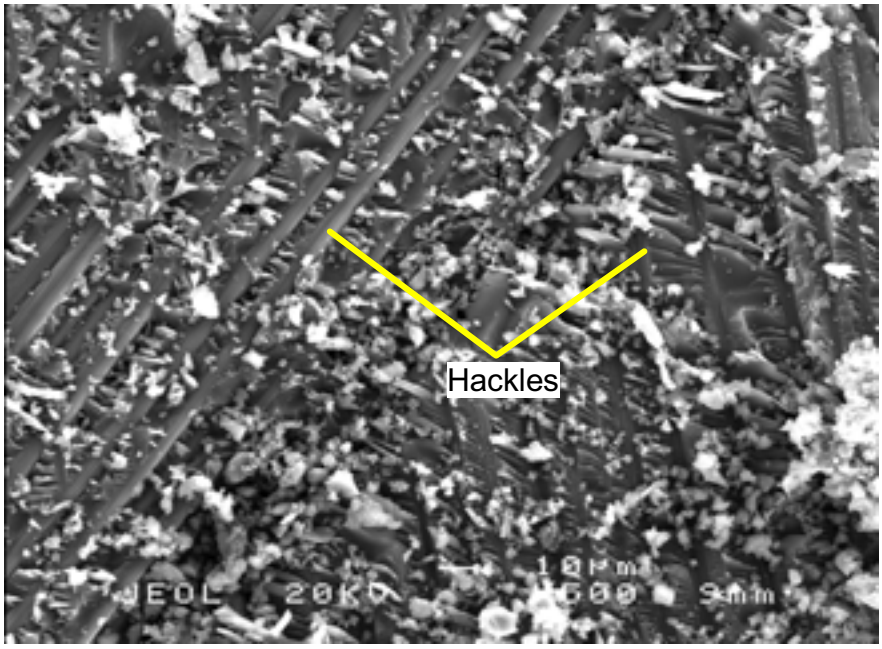

ImageNo: 208A0606, Project No:A00415 — 50 µm

Figure 36. Example SEM photograph from the top forward area of specimen LA1a. Hackles are indicated between +45-degree fibers (left) and zero-degree imprints (right), pointing up and forward. Orientation as in figure 35.

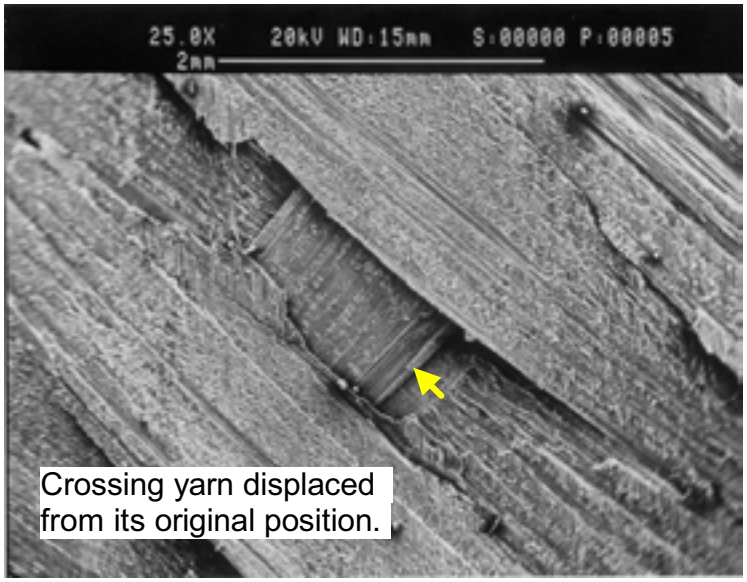

Figure 37. Specimen LA5 inner surface. An unlabeled arrow indicates a crossing bundle that was displaced from its original position. Orientation as in figure 35.

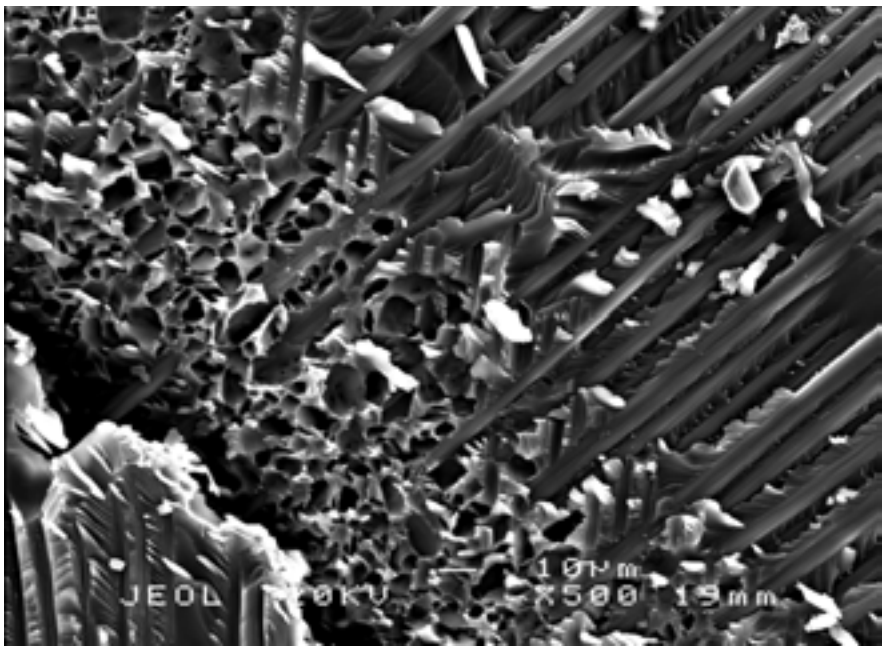

Figure 38. Microscopic matrix porosity in a region where bundles cross on specimen LA1b. The main bundle is at the upper right, and vertical imprints are at the lower left. Orientation as in figure 35.

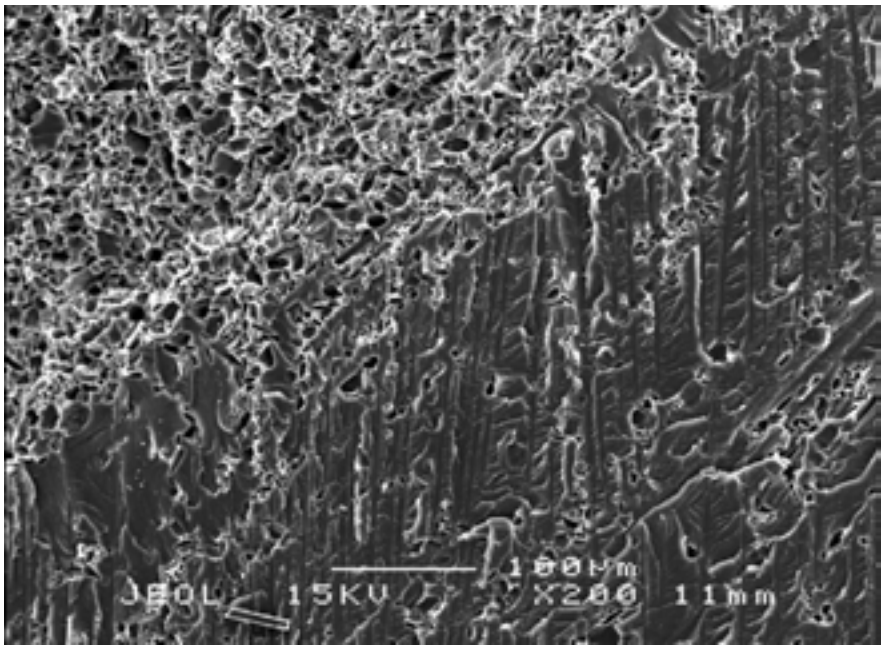

ImageNo:209A0861, Project No:A00415 200 μm

Figure 39. Microscopic matrix porosity on the outboard piece of LA1c. This porosity is shown at the upper left, with ill-defined hackles shown at the lower right. Orientation as in figure 35.

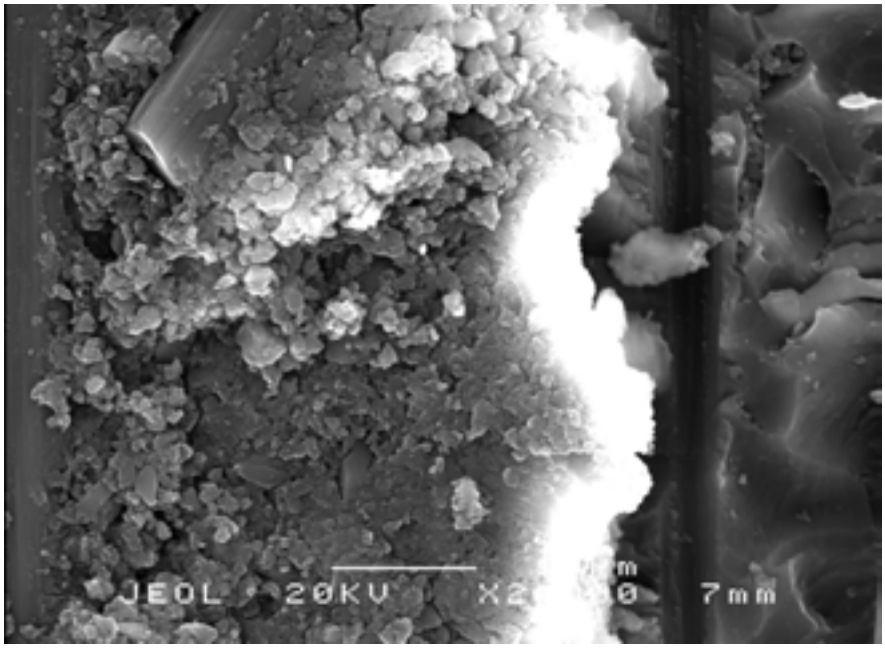

ImageNo: 209A0858, Project No:A00415 20 μm

Figure 40. Microscopic matrix granularity on the outboard piece of LA1c. A fiber fragment is shown at the upper left. Orientation as in figure 35.

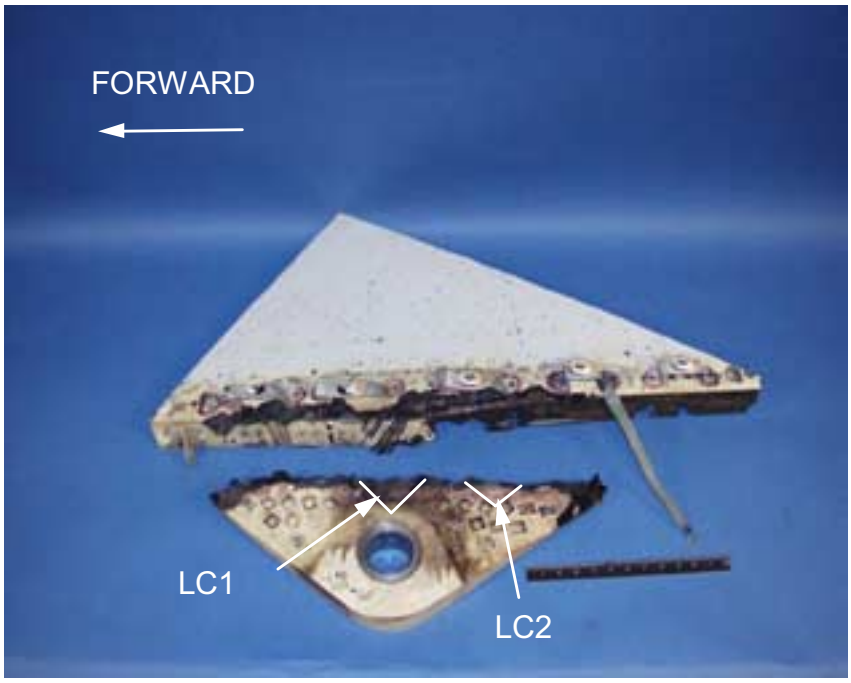

ImageNo:209A0587, Project No:A00387

Figure 41. Overall view of the two portions of the fractured structure at the left center lug viewed looking from the left.

ImageNo: 209A0602, Project No:A00387

Figure 42. Upper fracture surface at the left center lug, viewed looking upward parallel to zero-degree fibers.

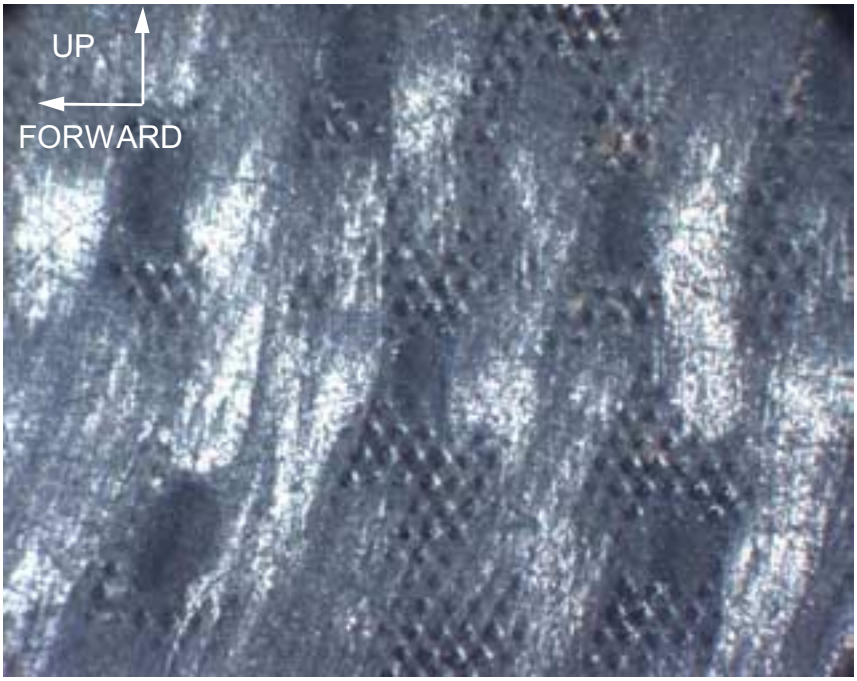

Figure 43. Interlaminar fracture surface on the inboard piece of specimen LC2.

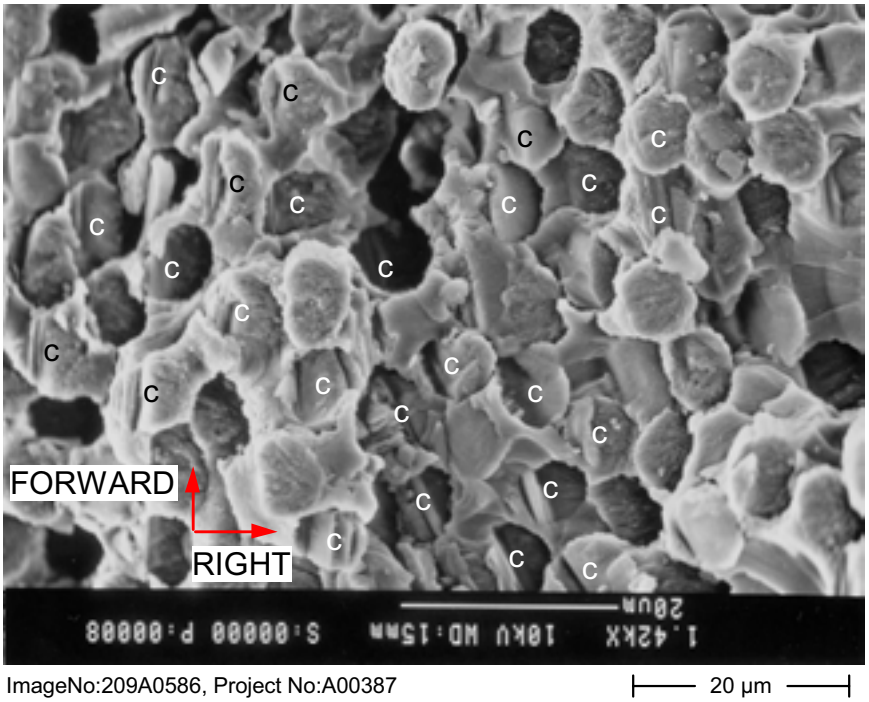

Figure 44. Translaminar fracture surface on the outboard piece from specimen LC2, with the fibers indicated by "c" containing chop marks typical of compressive failure.

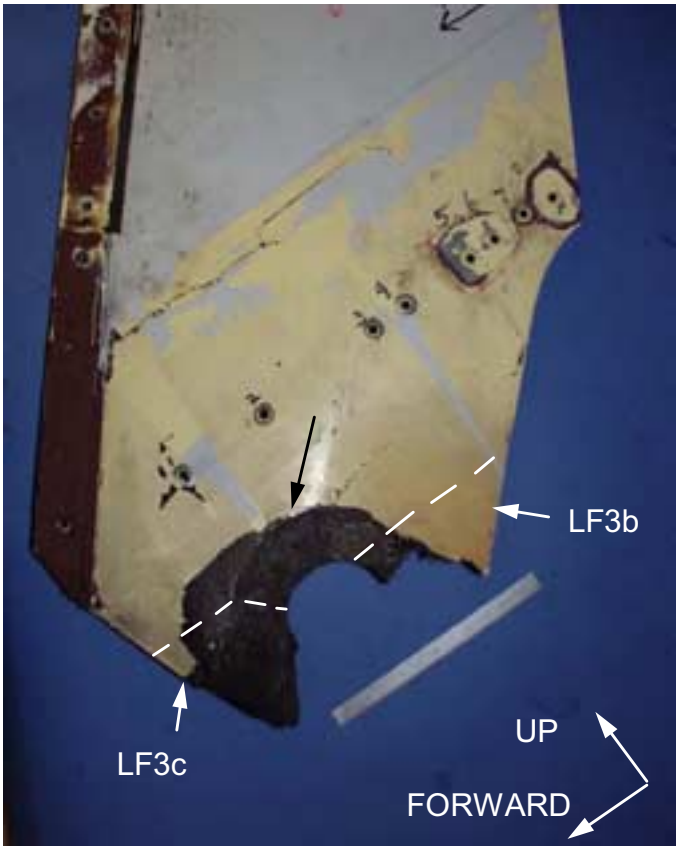

ImageNo:210A0041, Project No:A00387

Figure 45. Overall view of the left forward lug translaminar fracture. An unlabeled arrow indicates the upper end of the bearing indentation.

ImageNo:210A0046, Project No:A00387

Figure 46. Upper fracture surface of the left forward lug, viewed looking up.

ImageNo:210A0045, Project No:A00387

Figure 47. View of the aft surface of the left forward lug.

ImageNo: 210A0043, Project No:A00387

Figure 48. View of the forward surface of the left forward lug.

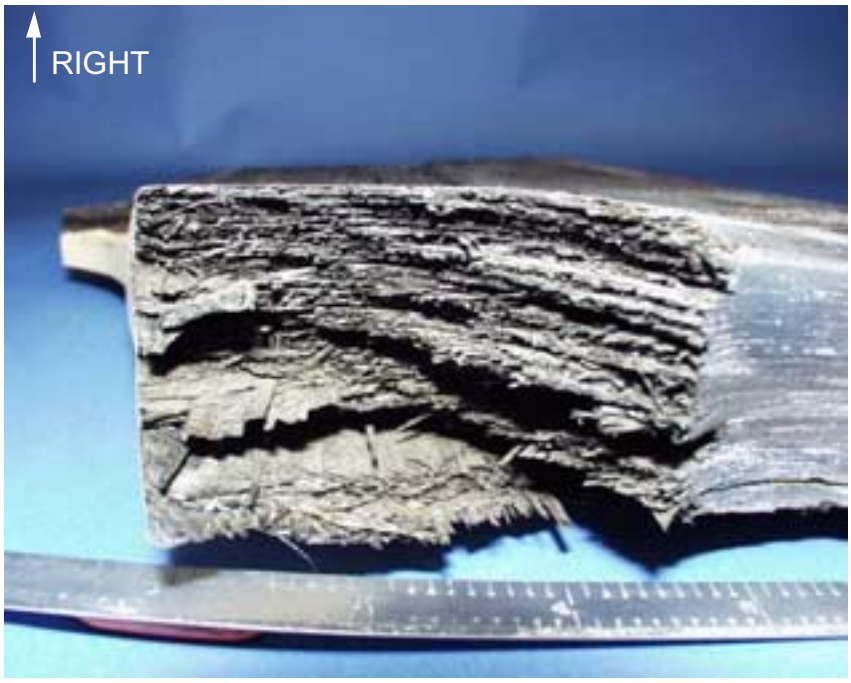

ImageNo:210A0044, Project No:A00387

Figure 49. Closer view of the left forward lug upper fracture surface, aft leg, as viewed looking upward parallel to the zero-degree fiber direction.

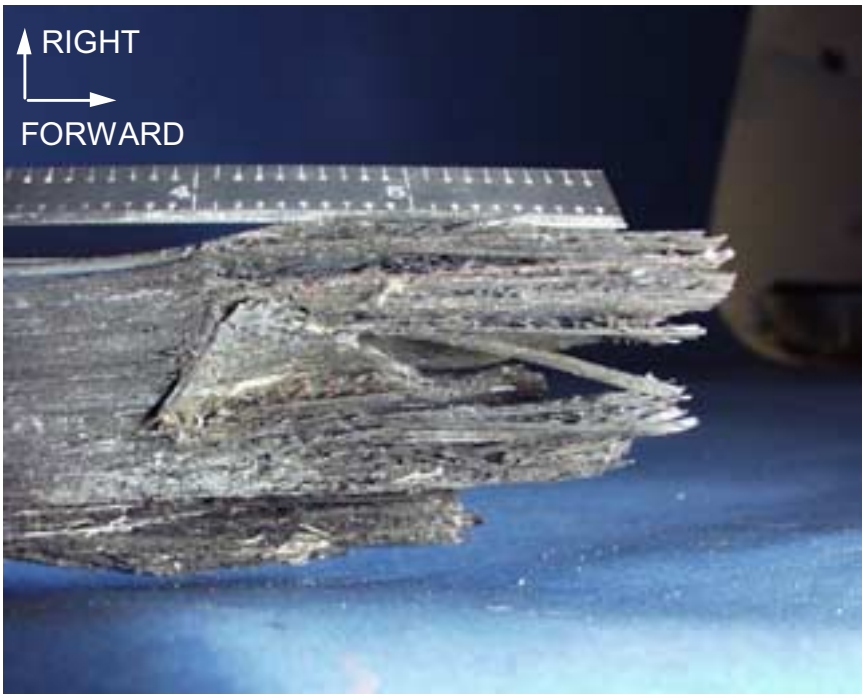

ImageNo: 210A0042, Project No:A00387

Figure 50. Closer view of the left forward lug upper fracture surface, forward leg, as viewed looking up.

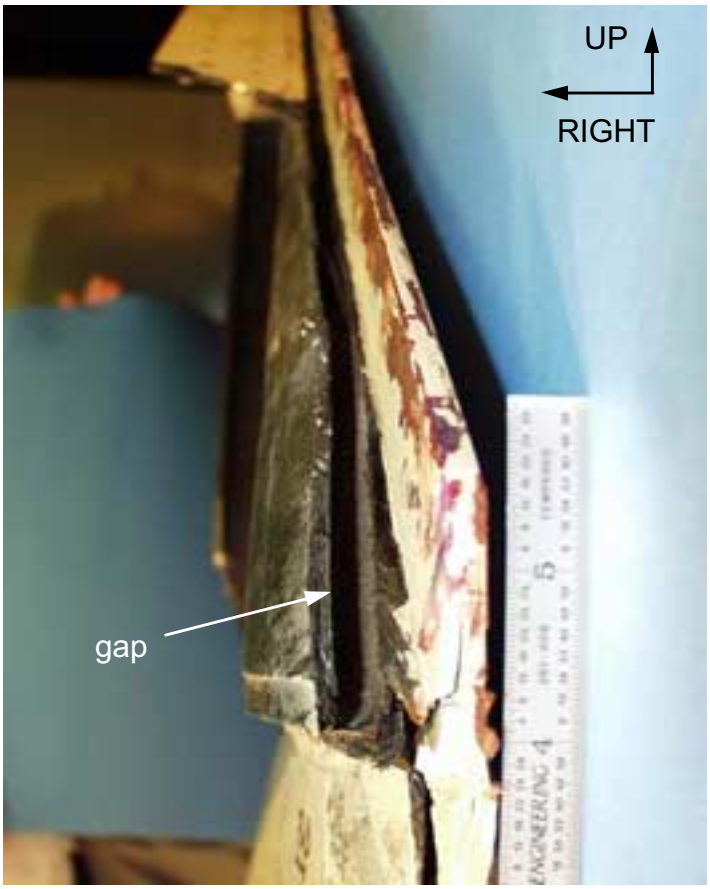

ImageNo: 210A0071, Project No:A00387

Figure 51. The visible gap at the forward lower end between the inner precured lug structure and the stringer outer flange structure as viewed looking aft.

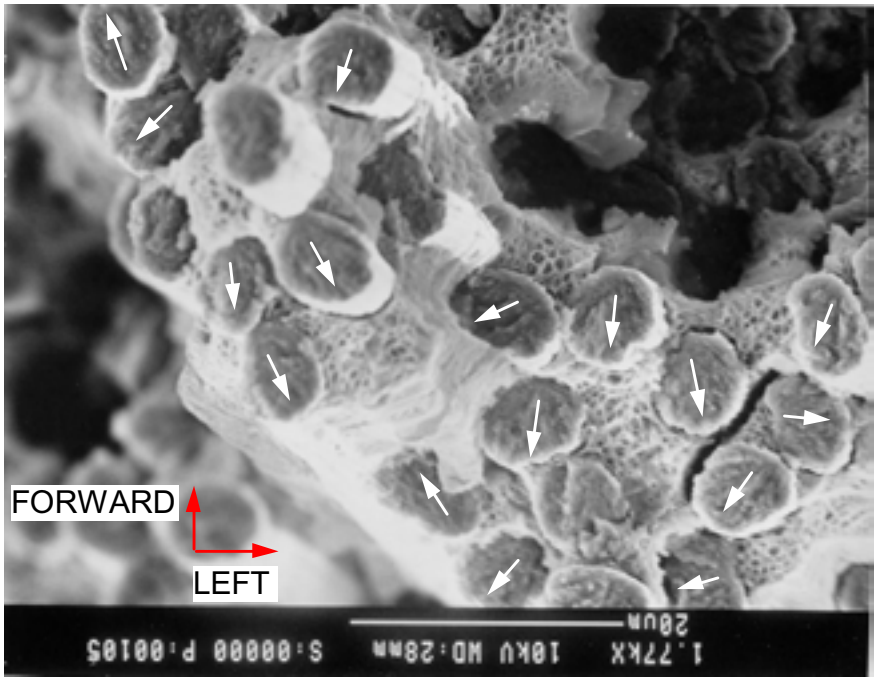

ImageNo:210A0078, Project No:A00387 20 µm

Figure 52. SEM photograph of the ends of zero-degree fibers from specimen LF3b. Arrows indicate fracture propagation direction in fibers with radial marks.

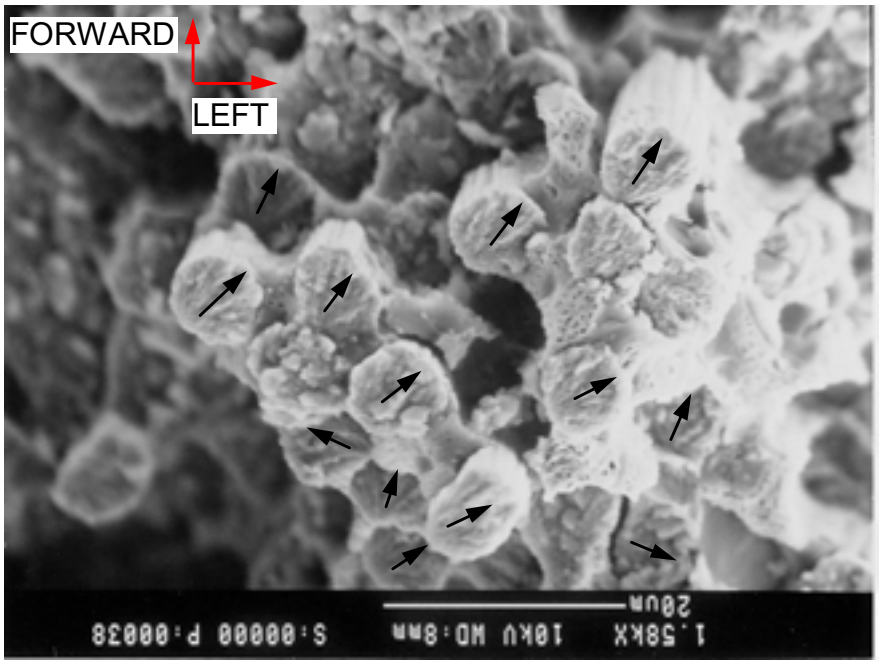

ImageNo: 210A0078, Project No:A00387 20 µm

Figure 53. SEM photograph with arrows indicating the direction of tensile crack propagation on the ends of zero-degree fibers from the inboard center piece of specimen LF3c.

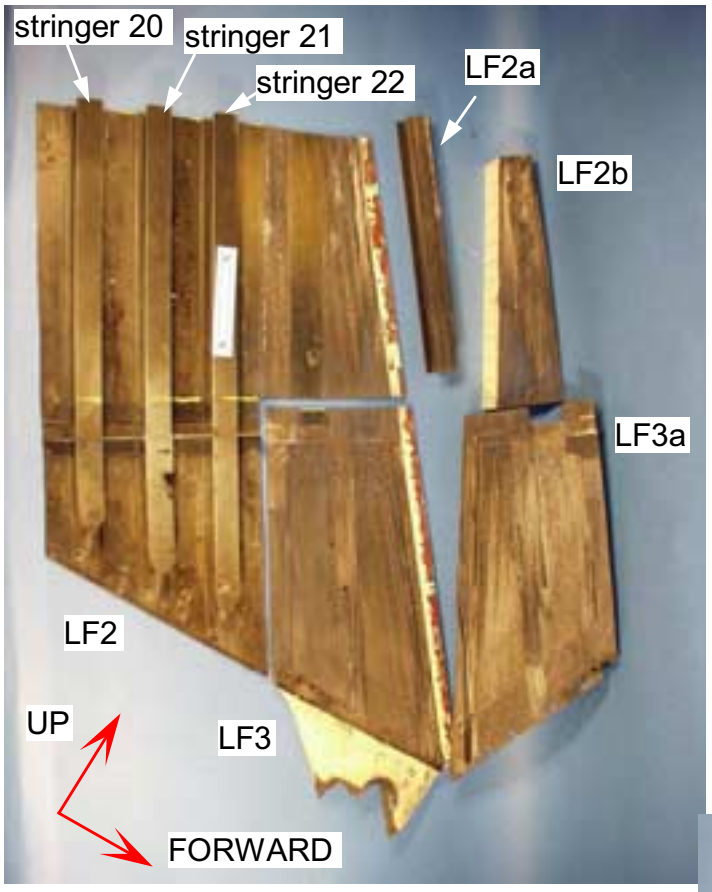

ImageNo:210A0031, Project No:A00424

Figure 54. Mating pieces after cutting to expose the interlaminar fracture above the left front lug. Arrows indicate UP and FORWARD for the main pieces LF2 and LF3.

Figure 55. Specimens cut from section LF3a for examination in the SEM.

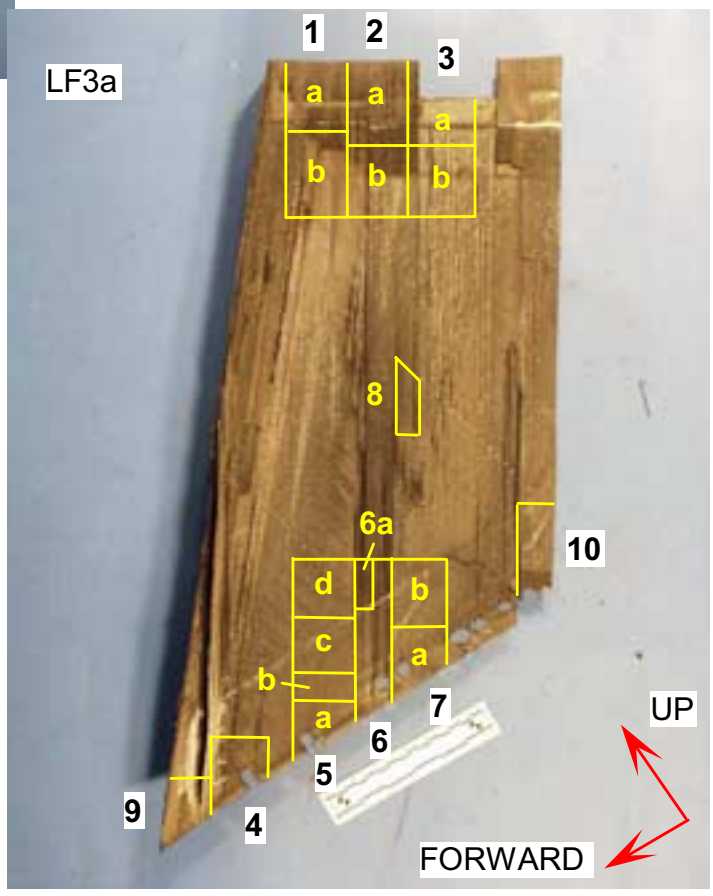

ImageNo: 210A0032, Project No:A00424

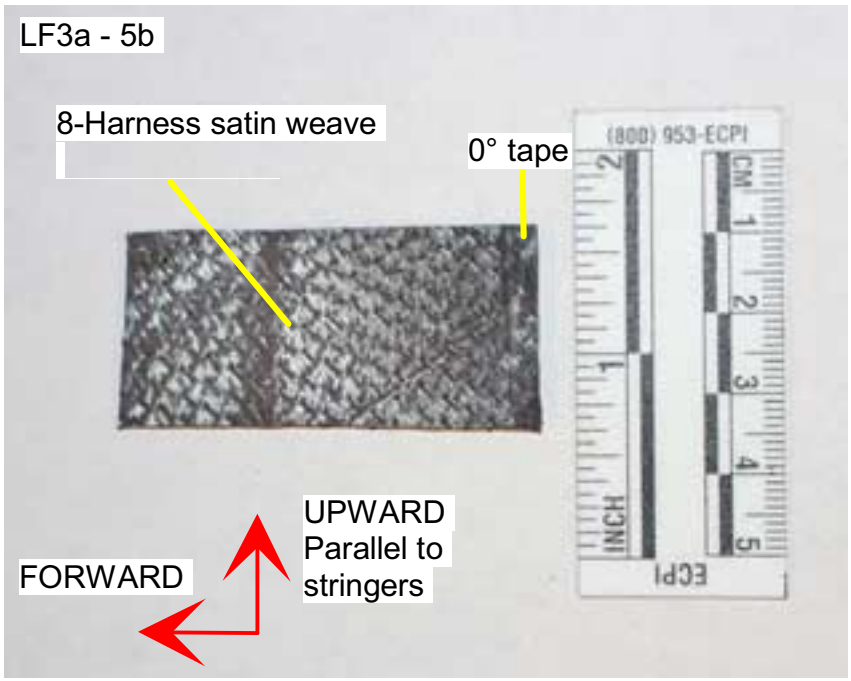

ImageNo:209A0603, Project No:A00424

Figure 56. Fracture surface from specimen LF3a-5b.

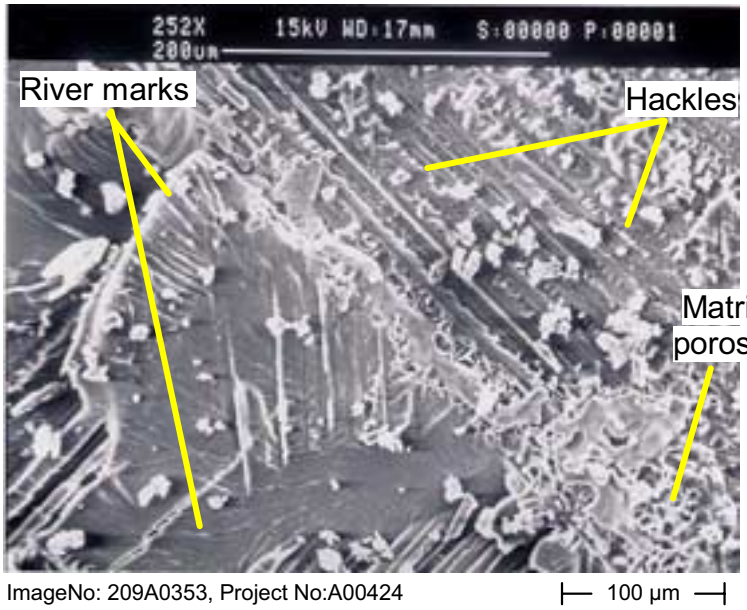

ImageNo: 209A0353, Project No:A00424

Figure 57. Example SEM photograph from the top forward corner of specimen LF3a-5b. Hackles indicated point up and forward, and river marks also point generally up and forward. Orientation as in figure 56.

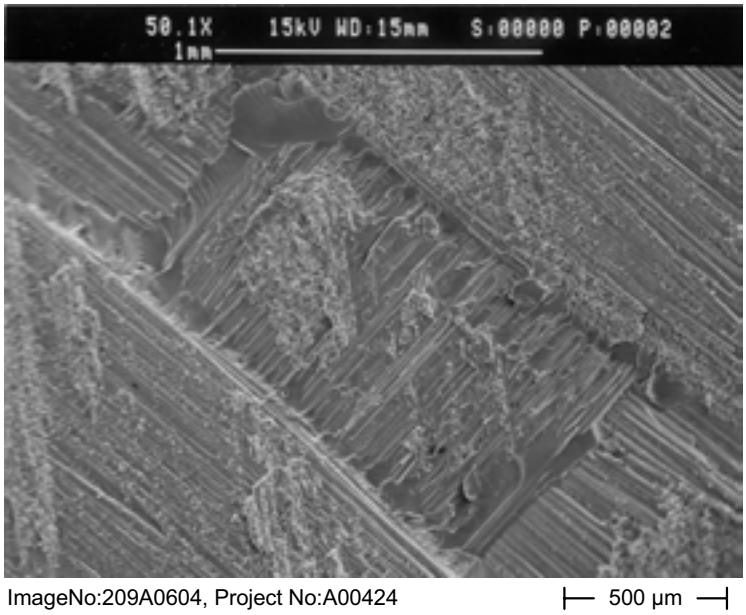

Figure 58. A view of the center of specimen LF3a-5c showing a bundle crossing in the woven fabric. Orientation as in figure 56.

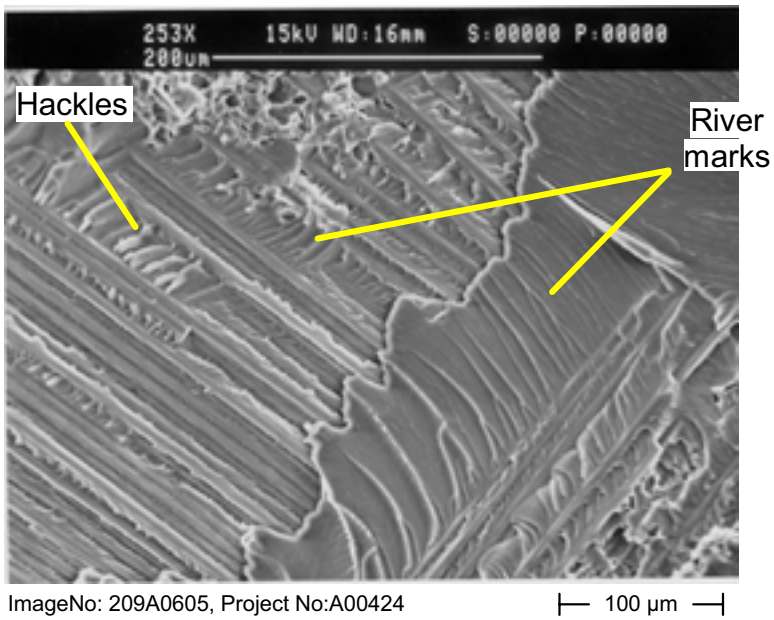

Figure 59. Higher magnification view of the upper left corner of the bundle crossing shown in figure 58. Orientation as in figure 56.

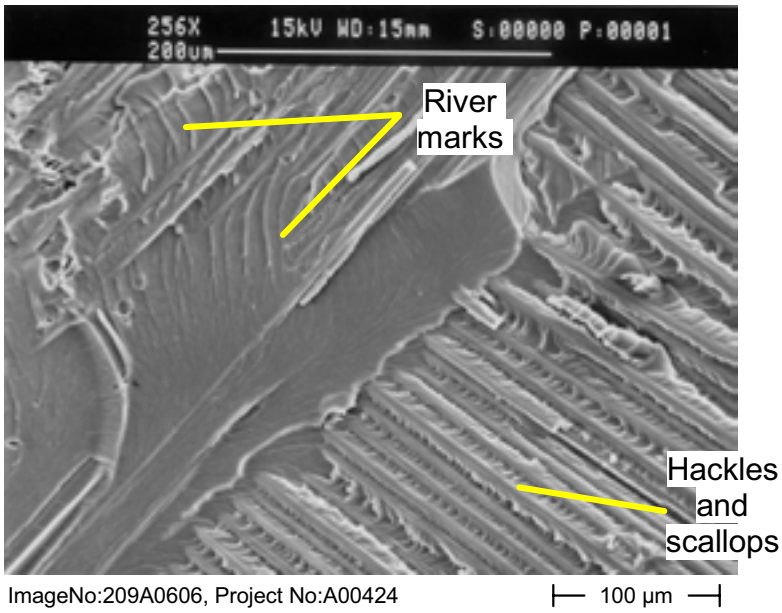

Figure 60. Higher magnification view of the lower right corner of the bundle crossing shown in figure 58. Orientation as in figure 56.

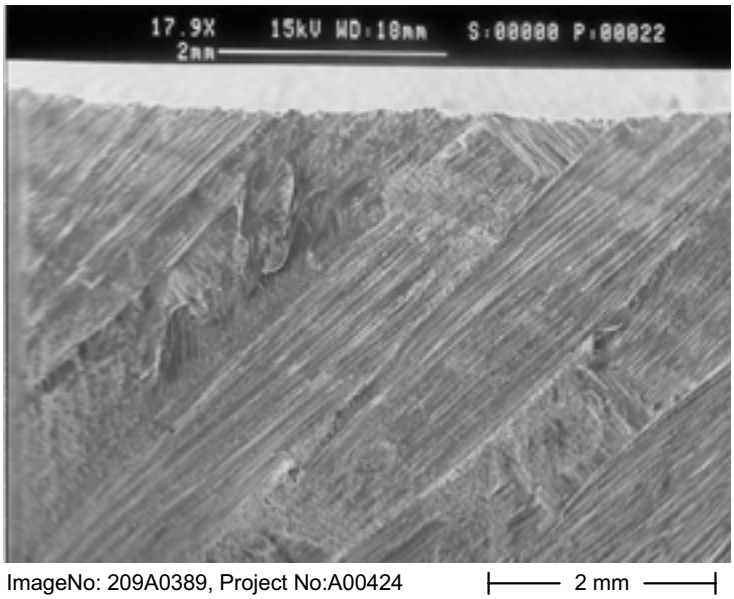

Figure 61. Faint bands at the top forward edge of section LF2b-1 indicate the direction of crack propagation upward and aft. Orientation as in figure 56.